Arbetsrapport

Org enh. och nr: AE FR-113

Titel och författare

Reactor physics measurements on $ThO_2/U^{235}O_2$ fuel assemblies in RO

R. Persson, A.J.W. Andersson, S. Grifoni*, C. Schittenhelm**, E.K. Sokolowski, and V. Tosi*

AE doc reg

Org enh och nr: AE-FFR-113

Antal original sid: /38

24 Figs.

Datum: 2.11 1967

Godkänd av

Rapportens sv/tv, uppdragsgivare e. d.

This material has been copied under licence from CANCOPY. Resale or further copying of this material is strictly prohibited.

Le présent document a été reproduit avec l'autorisation de CANCOPY. La revente ou la reproduction ultérieure en sont strictement interdites.

Utsändes till

FD	1 ex
FTB-Sthlm	1 ex
FTB Studsvik	2 ex

Summary

According to an agreement between CNEN, the Halden Project and AB Atomenergi reactor physics experiments on ThO_2 fuel assemblies with 2 % $U^{235}O_2$ were undertaken in RO during April 1967. Bucklings, flux peaking at fuel gaps, spectral indices and conversion ratios were measured both with D_2O and with air as "coolant" in the 7-rod clusters. Since only seven clusters were available the material buckling had to be determined by the progressive substitution technique. Bucklings were measured in four lattices (hexagonal pitch 11, 13, 15, and 17 cm), whereas the other quantities were studied only in the largest test region of two lattices (13 and 17 cm). Small quality variations between the fuel assemblies gave significant contributions to systematic errors in the buckling measurements. Only for the largest lattice pitch, i.e. 17 cm, deviations from asymptotic spectral conditions were of minor importance in the central test assembly. The RO measurements were performed prior to high-power runs of the ThO_2 fuel assemblies in HBWR (Halden).

* CNEN

** Halden Project

List of contents

		page
1.	Introduction	1
2.	Fuel data	1
3.	Codes utilized in calculations	2
4.	Buckling studies	3
4.1	Experimental technique	3
4.2	Method of evaluation	3
4.3	Results	6
4.3.1	Reference cores	6
4.3.2	$\delta D/D$ measurements	7
4.3.3	Progressive substitutions with ThO_2	8
5.	Measurements of the flux peaking around the fuel gap	10
5.1	Scope of work	10
5.2	Experimental technique	11
5.3	Results	11
6.	Calculations of the gap effect	13
7.	Spectrum index measurements	15
7.1	Scope of work	15
7.2	Experimental conditions	16
7.3	Spectrum index correlations	16
7.4	Results	17
8.	Conversion ratio measurements	18
8.1	Scope of work	18
8.2	Experimental technique	19
8.3	Results	21
8.4	Recommendations for future measurements	22
9.	Conclusions	23
10.	Acknowledgements	24

References

Table I - XIII

Figures

1. Introduction

According to a trilateral agreement between CNEN (Italy), the Halden Project and AB Atomenergi reactor physics measurements were undertaken in the RO critical facility on ThO_2(2 % $U^{235}O_2$) fuel assemblies prior to their use in HBWR. The experiments were performed during the last three weeks in April 1967. Material bucklings, axial flux peaking, spectral indices and conversion ratios were studied. Only seven fuel assemblies were available, so the progressive substitution technique had to be applied for the bucklings measurements. The other quantities were investigated only in the largest test region of seven fuel assemblies. Four different pitches were studied, viz. 11, 13, 15, and 17 cm (hexagonal lattice), corresponding to moderator-to-fuel volume ratios from 10.5 to 27.2. The effect of loss of coolant was investigated by using empty as well as D_2O-filled channels in all the cases.

2. Fuel data

Pellets

Composition:	97.6 w/o ThO_2 2.0 w/o $U^{235}O_2$ 0.4 w/o $U^{238}O_2$
Diameter:	12.59 mm
Length:	20 and 40 mm. (Special pellets were manufactured for length adjustments and for activation experiments).
Density:	9.57 ± 0.02 (based on the weight per unit length of fuel and the nominal diameter).

Canning (zircaloy-2)

ID:	12.76 mm (13.00 mm in 4 special tubes for activation experiments)
OD:	13.96 mm

Stringer

Active length:	828.5 mm
Total length:	890.5 mm
Number:	98, incl. 4 special stringers with removable end plugs.

Fuel assembly

Geometry: 7-rod clusters, c-c: 23 mm (one rod = 2 stringer sections with a fuel gap of about 40 mm in the joint region)

Number: Seven, of which one was used for activation work having two rods easily removable.

Shroud tube (zircaloy-2)

ID: 71 mm

OD: 73 mm

Each shroud tube had a bottom closure provided with a pneumatic valve used in connection with void experiments.

See also fig. 1.

The fuel of the reference lattices was natural uranium metal, diameter 3.05 cm, canned in aluminium, ID 3.15 cm, OD 3.45 cm. In some cases spikes were used in the form of 31-rod clusters of UO_2 (1.2 % U^{235}), diameter 1.26 cm. In one case 27-rod clusters of UO_2 (natural), diameter 1.35 cm, were put into the reflector.

3. Codes utilized in calculations

When comparing the experimental results with theoretical models we have used the three cell programs

METHUSELAH (5 groups; origin: UKAEA) [1]
PLUTHARCO (four-factor formalism; origin: EURATOM) [2]
REBUS (four-factor formalism; origin: AB Atomenergi) [3]

and the macroscopic program

EQUIPOISE (2 groups, 2 dimensions) [4] .

Only buckling values were calculated by all the three cell programs. The axial and radial diffusion coefficients were obtained from REBUS in which program the Benoist [5] theory is used. The gap effect was studied by combining two-group constants from METHUSELAH with EQUIPOISE. Lu/Mn activity ratios as well as relative conversion ratios were calculated by METHUSELAH, whereas the theoretical r-values were obtained from PLUTHARCO.

4. Buckling studies

4.1 Experimental technique

The principles of the progressive substitution technique are described in ref. [6] and in the following only problems related to the present experiments are to be discussed. Since only seven ThO_2 fuel assemblies were available the hexagonal lattice was chosen as being most suitable.

Due to the length of the ThO_2 fuel assemblies the critical height was limited to 1.85 m (see fig. 1), which implies that the reference lattices had to have lower critical heights than that. For the 11 cm and 13 cm lattices enriched uranium oxide clusters were placed in the peripherical part of the core and in the reflector respectively in order to increase the effective (geometric) buckling of the system. These two complicated cores with seven ThO_2 fuel assemblies substituted in the center are shown in figs. 2 and 3. The buckling equivalences of the regions containing the UO_2 clusters were determined by complementary substitution experiments. The 11 cm (or, more precisely, $19/\sqrt{3}$ cm) reference lattice was obtained by adding rods to the primary 19 cm lattice stepwise according to fig. 4.

The substitution steps with ThO_2 fuel assemblies are shown in fig. 9. Eccentric test regions were allowed.

The D_2O level is measured within $\pm$ 0.01 cm (relative), which implies that the temperature had to be known to better than 0.03 ^{o}C. Assuming $\partial\rho/\partial T$ to be known ($\sim$ 25 pcm/^{o}C) we get dH/dT by means of $\partial\rho/\partial H$, e.g. obtained from period measurements.

No attempt was made to measure the reactivity effect of the fuel gap due to the limited length of the fuel assembly compared with the critical heights available. With a critical height of about 1 m it would have been possible to determine the reactivity effect of the gap by lowering one test element in the bottom hole at the center of the tank and in this way varying the axial statistical weight of the perturbation.

4.2 Method of evaluation

One-group perturbation theory combined with an unconventional cell definition was used for the analysis [6]. By placing the fuel in the

corners of a cell we get more kinds of cell than there are kinds of fuel and in that way we introduce a transition region.

In the simplest case, i.e. when D is constant, the one-group perturbation theory gives

$$B^2 = \sum_i B_i^2 W_i \tag{1}$$

where

$$W_i = c \int_{V_i} \phi_o \phi_i \, dV \tag{1a}$$

ϕ_o = the unperturbed flux,
ϕ_i = the actual (one-group) flux,
c = normalization constant ($\sum_i W_i = 1$) .

Eq. (1) can be rewritten as

$$B^2(n) - B^2_{ref} = \sum_i^{\substack{\text{outer}\\\text{regions}}} (B_i^2 - B^2_{ref}) W_i(n) + \sum_j^{\substack{\text{trans.}\\\text{regions}}} (B_j^2 - B^2_{ref}) W_j(n) + (B^2_{test} - B^2_{ref}) W_{test}(n) \tag{2}$$

where n is the number of test elements. Taking differences relative to the case n = 0 we get

$$B^2(n) - B^2(o) = \sum_i^{\substack{\text{outer}\\\text{regions}}} (B_i^2 - B^2_{ref})[W_i(n) - W_i(o)] + \sum_j^{\substack{\text{trans.}\\\text{regions}}} (B_j^2 - B^2_{ref}) W_j(n) + (B^2_{test} - B^2_{ref}) W_{test}(n) \tag{3}$$

If $W_i(n) = W_i(o)$ the outer regions should have no effect (except for the calculation of W_j and W_{test}). Owing to perturbed fluxes the first summation on the right-hand side of eq. (3) is usually different from zero but small.

In order to be able to represent eq. (3) in graphical form also in the case with two kinds of transition cells we assume that $(B_j^2 - B_{ref}^2)$ is a bilinear function of the number of test elements present in the various cells. We use $j = 1$ for a transition cell where only one test element is involved and $j = 2$ for a transition cell with test elements in two of the three corners. With this assumption we get

$$B_1^2 - B_{ref}^2 = \frac{1}{3}\,(B_{test}^2 - B_{ref}^2) + \delta B_t^2 \tag{4}$$

$$B_2^2 - B_{ref}^2 = \frac{2}{3}\,(B_{test}^2 - B_{ref}^2) + \delta B_t^2 \tag{5}$$

Eq. (3) can now be arranged in the form

$$\begin{aligned} B^2(n) - B^2(o) = & \sum_{i}^{\text{outer regions}} (B_i^2 - B_{ref}^2)\left[W_i(n) - W_i(o)\right] + \\ & + \delta B_t^2\,\left[W_1(n) + W_2(n)\right] + \\ & + (B_{test}^2 - B_{ref}^2)\,\overline{W} \end{aligned} \tag{6}$$

where

$$\overline{W} = \frac{1}{3}\,W_1 + \frac{2}{3}\,W_2 + W_{test} \tag{7}$$

If the outer regions can be neglected eq. (6) says that $\left[B^2(n) - B^2(o)\right]/\overline{W}$ is a linear function of $\left[W_1(n) + W_2(n)\right]/\overline{W}$. The intercept is $(B_{test}^2 - B_{ref}^2)$ and the slope is equal to δB_t^2.

In the general case when D is different in different regions and different directions we have [6]

$$\sum_k \sum_i \left[D_{ki}\,(B_{ki}^2 - B_{ko}^2)\,W_i - D_{ki}\,B_{ko}^2\,\Omega_{ki}\right] = 0 \tag{8}$$

where

$$\Omega_{ki} = \int (\nabla_k \phi_o)\phi_i \, d\underline{S}_{ki} \Big/ B_{ko}^2 \sum_i \int \phi_o \phi_i \, dV \qquad (9)$$

$k = r$ and z,

o refers to the geometrical buckling of the whole system.

Since the weight functions W_i and Ω_{ki} have quite different spatial dependence, we are able to determine their coefficients separately by varying the size or/and position of the perturbation in a suitable way. It means that we are able to find D/D_{ref} as well as B^2 experimentally [7].

The evaluation of the measurements was made by means of the computer program SIMBA [8]. The regions of triangular cells were transformed to circular regions by a special program [9].

4.3 Results

4.3.1 Reference cores

The 15 cm and 17 cm reference cores were quite clean but surrounded by a D_2O reflector. Continuing the triangular cell pattern out in the reflector we introduced two kinds of transition cells between core and reflector. Assuming the buckling of a cell to be a unique function of the fuel-to-moderator volume ratio we can ascribe buckling values to the transition cells. That assumption seems to be plausible according to the experimental results shown in fig. 14 of ref. [6].

The 13 cm reference core was somewhat more complicated (see fig. 3). As mentioned before, uranium oxide clusters were placed in the reflector in order to lower the critical height. The effective buckling of the homogenized outermost region was determined by substitution measurements (see Table V).

The 11 cm reference core was most complicated as can be seen from fig. 2. The starting point was the pure 19 cm lattice. In the first step 24 of the outer rods were replaced by six enriched uranium oxide clusters. Then metal rods were added in the center of the core in successive steps (see fig. 4). The experimental values are given in Table I.

In order to interprete this experiment in the best way we tried different kinds of transition regions. If one defines a test cell and a reference cell as shown in fig. 4 no transition region will be introduced. Since this approach does not work with the method of analysis applied here, a transition cell was defined as is also shown in fig. 4. However, with such a cell definition, which gave $B^2_{test} = 6.972 \pm 0.093\ m^{-2}$, the thickness of the transition region varies considerably with the size of the test region as shown in fig. 5. We therefore also interpreted the measurements by using annular transition regions of constant thickness for all substitution steps, the thickness being equal to that of the one-element substitution in the preceding case. Since this interpretation, which may be regarded as the other extreme case, and which gave $B^2_{test} = 6.547 \pm 0.165\ m^{-2}$, changed the sign of the differences (still large) between experimental and fitted critical heights, we assumed as a third case that the thickness of each transition region was the mean of the two extreme cases. This case gave $B^2_{test} = 6.707 \pm 0.028\ m^{-2}$. The goodness of the three different interpretations are illustrated in the insert of fig. 5. The best choice for the transition region thicknesses is obviously the one that minimizes the differences between the fitted and experimental critical heights for the various substitution steps. One can see from fig. 5 that this choice is rather close to the intermediate case. With interpolated values for the thicknesses of the transition regions we obtain the results which are given in Table I.

It may be observed that although the bucklings of the 19 cm and $19/\sqrt{3}$ cm reference lattices are very close, the critical heights for the various substitution steps are lower, due to the presence of the transition region which has a larger material buckling.

4.3.2 $\delta D/D$ measurements

The substitution measurements for the $\delta D/D$ determinations were made in the 17 cm reference lattice by means of a single ThO_2 fuel assembly. For the $\delta D_z/D$ measurements the test fuel assembly was placed in the central position and the void depth was varied, whereas for the $\delta D_r/D$ measurements the fuel assembly was placed in various radial positions and in each case the "coolant" was changed from air to D_2O. The effect of $\delta D/D \neq 0$ is that the buckling change is no longer proportional to

$\int\phi^2 dV$ only, but terms proportional to $\int(\nabla\phi)^2 dV$ are also present. The experimental values are given in Tables II and III and evaluated graphically in figs. 6 and 7. The function $(\delta D/D)V_{cell}$ should be rather independent of the lattice pitch as is also shown in fig. 8 where the experimental results are plotted together with those from REBUS [3] calculations and from a simple semi-empirical formula [10].

As regards spectral conditions the experimental values of $\delta D/D$ can be assumed to be related to a test pitch which is larger (by about 25 %) than that of the reference lattice, since for the same lattice pitch the absorption is smaller in a reference cell than in a test cell. Further we can assume that the interaction between adjacent voided channels in an infinite lattice can be neglected, since the pitch is sufficiently large. The experimental $\delta D/D$ values may consequently be compared with theoretical values valid for a test pitch of approximately 21 cm.

4.3.3 Progressive substitutions with ThO_2

The various ThO_2 fuel assemblies were first intercompared in a 13 cm reference lattice. Unfortunately this was not the most sensitive lattice, but the 17 cm lattice would have been better in that respect. The results are given in Table IV. There were small but significant differences in quality between different fuel assemblies. The special fuel assembly used for activation experiments deviated most (about 10 pcm) from the mean value.

The substitution steps and the cell assumptions used in connection with the ThO_2 fuel assemblies are shown in fig. 9. Two different cell definitions were considered. The first of them, with equilateral triangular cells and two kinds of transition cells, is shown in the substitution steps on the left-hand side of fig. 9. The second method, with rhombic cells and only one kind of transition cells, is shown in the substitution steps on the right-hand side of fig. 9.

The experimental critical heights are given in Tables V and VI and they are also plotted in fig. 10 versus the number of substituted elements. We observe that the difference between the critical heights of the air- and water-cooled cases seems to be reliable within about 0.2 mm, judging from the fit to the curves in fig. 10, whereas the

critical heights of the separate cases are not such smooth functions of the number (n) of substituted fuel assemblies. The fluctuations are, however, with some exceptions (mainly one point for the 15 cm pitch), well correlated to the differences between the properties of the fuel assemblies as is displayed in Table IV. We made correlation studies based on the assumption that for each pitch the adjusted critical heights should be a smooth function of n . Consequently we may write

$$H_{adj}(n) = H(n) - C \sum_{i=1}^{n} \Delta H(i) \tag{10}$$

where

$H(n)$ = experimental critical height with $\underline{n}$ elements substituted,

$\Delta H(i)$ = critical height obtained in the intercomparison experiments for element $\underline{i}$ minus a suitable average height (see Table IV),

C = correlation constant depending on the lattice pitch.

By assuming $H_{adj}(n) = H(o) + an + bn^2$ we found the following values of C:

0.6, 0.9, 1.85, and 2.75

for the 11, 13, 15, and 17 cm lattice pitches, respectively. The uncertainty in C is approximately $\pm$ 0.5. The ThO_2 fuel assemblies were in all lattices inserted in the same order as given in Table IV.

Eq. (6), which is based on the assumption of two kinds of transition regions correlated according to eqs. (4) and (5), has been used for graphical representation of the measurements with D_2O coolant in fig. 11. The correlation constant C was neglected. The notation W_{trans} is equal to $W_1(n) + W_2(n)$ in eq. (6). δB_{corr} means that the contributions from the outer regions are taken into account. We notice from fig. 11 that substitutions with one and two fuel assemblies usually do not fit to the assumption on which eq. (6) is based, viz. that the buckling of the transition cells is a bilinear function of the number of test elements connected with the cell definition (see fig. 9). If

we assume no interrelation between the bucklings of the two kinds of transition cells, we get the SIMBA results shown as extrapolated values in fig. 11.

All the material bucklings obtained in the analysis by means of SIMBA are collected in Table VII. The bucklings with air-filled assemblies, i.e. anisotropic cases, have been adjusted to a geometry where $B_r^2 = 2B_z^2$. As said before two kinds of cell definition were used and the effect of the fuel quality correction was investigated. When comparing the results of the two cell definitions we see a small systematic trend, but it is least pronounced in the cases where the fuel quality correction has been applied. The test bucklings obtained with two kinds of transition regions are thought to be most correct. These results together with the bucklings of the transition regions are plotted in fig. 12. Since the absolute values of the bucklings of the transition regions are of an expected magnitude, we conclude that the cell size is reasonable.

Fig. 13 shows theoretical results obtained from METHUSELAH (only D_2O coolant), PLUTHARCO and REBUS (mark 1). A second version of REBUS, where $T_n \neq T_m$ should be used [11], gives approximately the same bucklings. The predictions by REBUS are most off, whereas PLUTHARCO does not give the correct dependence on the lattice pitch.

Fig. 14 demonstrates that the buckling change caused by emptying the coolant channels is rather well predicted by REBUS and PLUTHARCO for the 13 cm lattice.

The uncertainty caused by a systematic error of 1.0 cm in the critical heights is $<0.08\ m^{-2}$ in the individual bucklings and $<0.03\ m^{-2}$ in $B^2_{test} - B^2_{ref}$.

5. Measurements of the flux peaking around the fuel gap

5.1 Scope of work

In the joint between the upper and lower stringers there was an axial gap of about 40 mm in the fuel. The material in this gap region including a spacer plate was mainly zircaloy-2. The aim of the experiment described here was to determine the flux (power) peaking around the spacer region. While measurements were performed at both 13 and 17 cm lattice pitches, only results from the first case will be given here, since the 13 cm lattice pitch is the same as in HBWR.

5.2 Experimental technique

We measured the thermal flux in an outer and an inner stringer both in the upper and in the lower part of the assembly, which was placed in the center of the test zone of seven fuel assemblies. Air as well as D_2O was used as coolant.

Copper foils, 0.1 mm thick, were used as detectors. In order to protect them from fission products, they were covered by 0.05 mm thick foils of copper (catcher foils). The counting was started not earlier then 12 hours after each irradiation, so only the Cu^{64} activity had to be considered (half life 12.8 h, whereas Cu^{66} has 5.1 minutes).

The activity of the Cu foils was counted in a back-and-forth sequence (1, 2, ..., n-1, n; n, n-1, ..., 2, 1), this cycle being repeated continuously until the desired statistics was obtained. The counting periods used were constant (30 sec.) and a constant interval (15 sec.) allowed for sample changing and punching of tape. In view of the selected sequence in the foil counting, and owing to the long half life of Cu^{64} the average of the two countings of one foil within the cycle can be considered as related to the same time for all foils [12].

5.3 Results

The resulting foil activities as a function of the foil positions are shown in figs. 15 and 16.

The purpose of the subsequent analysis is to evaluate the peaking factor, i.e. the ratio between the measured reaction rate distribution of a 1/v absorber and the unperturbed cosine flux. We have to consider the resonance absorption since copper is not a pure 1/v absorber. If we assume that the epithermal non-1/v contribution is not affected by the gap, i.e. is equal to $E \cos \alpha z$, we get

$$Q = \frac{Y - E \cos \alpha z}{A \cos \alpha z - E \cos \alpha z} \tag{11}$$

or

$$Q - 1 = \frac{(Y/A \cos \alpha z) - 1}{1 - E/A} \tag{12}$$

Here Y denotes the measured distribution along the stringers and Q the (neutron density) peaking factor. As 1 - E/A is equal to the 1/v activity divided by the total activity, we put

$$1 - E/A = f_{1/v} \tag{13}$$

where

$$f_{1/v} = \frac{1}{1 + rs} \tag{14}$$

is the resonance correction factor according to the Westcott formalism [13].

The epithermal spectrum index r is practically equal to the fraction of the neutron density belonging to the epithermal distribution. The parameter s is characteristic for the actual absorber, Cu, and is a function of the neutron temperature.

Equation (12) can thus be written as

$$Q = [(Y/A \cos \alpha z) - 1]/f_{1/v} + 1 \tag{15}$$

The value of $f_{1/v}$ (= 0.952) was obtained from spectrum index measurements (see section 7 below).

Plots of Q versus axial position are shown in figs. 17 and 18. The uncertainty in the position of the foils relative to the central spacer is negligible. The values of Q at the gap-fuel interface are given in Table VIII.

The fact that the (Q-1) values are 5-6 % higher at the lower end than at the upper end of the gap can be explained by the presence of a 5 mm air gap in the lower stringer(for free thermal expansion of the fuel). Even if the Q values are higher for the inner stringers, the absolute flux level is higher in the outer stringers, as shown in figs. 15 and 16 due to the radial flux depression across the fuel cluster. It can be noted that with air coolant the Q values are lower than with D_2O coolant.

6. Calculations of the gap effect

In the calculations of material buckling performed with the METHUSELAH and PLUTHARCO codes it was assumed that the gap discontinuity does not exist (in REBUS calculations the gap was homogenized along the fuel pin by suitably reducing the fuel density).

In order to see what correction should be applied to the measured values of the buckling, calculations were performed with the EQUIPOISE code to evaluate the effect of the gap. We assumed in these calculations that the presence of the gap brings about a change only in the axial buckling while the radial leakage is not affected. Therefore we considered a cell with zero radial leakage, while in the axial direction the correct dimension of the reactor was used.

We had to employ a two-dimensional code because, in order to have a more accurate result, we kept the cluster region separate from the moderator region. We obtained the two-group constants for the various regions of the cell from METHUSELAH calculations and we made a calculation for the real element with the gap as well as for an ideal element without the gap. We studied both the 13 cm and the 17 cm pitch cases with D_2O coolant. The thin bottom reflector was substituted by the extrapolated length in order to simplify the calculation, and for the reactor height an average from the progressive substitution steps was taken.

To take care of the increased absorption near the gap, a correction to the fast absorption cross section was introduced in the fuel region close to the gap. For this correction results reported in [14] were used with the S/M values relative to the fuel in this region and in the ideal infinite rod. In order to evaluate the change in buckling we consider the two-group expression

$$k_{eff} = \frac{k_{\infty 1}}{1 + \tau B^2} + \frac{k_{\infty 2}}{(1 + \tau B^2)(1 + L^2 B^2)} \qquad (16)$$

where

$$k_{\infty_1} = \frac{\nu\Sigma_{f_1}}{\Sigma_{rem} + \Sigma_{a_1}} \tag{17}$$

$$k_{\infty_2} = \frac{\nu\Sigma_{f_2}}{\Sigma_{a_2}} \; \frac{\Sigma_{rem}}{\Sigma_{rem} + \Sigma_{a_1}} \tag{18}$$

Here B^2 represents only the axial leakage. In the two cases with gap and without gap we obtain from the calculations two different k_{eff} values, which we convert to B^2 values according to expression (16). The k_{∞_1}, k_{∞_2}, L^2 and τ values are those for the unperturbed lattice in both cases. The difference in B^2 gives the correction we should apply. In Table IX the results are given.

In the 13 cm case the effect is very small because the core is undermoderated, so that the loss of fuel in the gap region is partly compensated by the increased resonance absorption in the fuel adjacent to the gap. The 17 cm case is overmoderated so that in this case the two effects contribute to decrease the buckling. By plotting the δB^2 values as a function of V_m/V_f and extrapolating linearly for the other cases which were not calculated, we obtain the corrections given in parenthesis (Table IX).

Due to the small magnitude of the correction we feel that the linear extrapolation is sufficient and that the different axial positions of the perturbation in the different experiments are unimportant.

In fig. 19 we have plotted the axial thermal flux distributions in the central pin and in the outer pin for the 13 cm pitch with D_2O coolant. When comparing the results to the measured distributions (see section 5 above), the following two things must be considered:

a) The fuel, cladding and coolant are homogenized in the calculation, so that the flux depression in the fuel with respect to the average in (fuel + cladding + coolant) is not taken into account. This flux depression is obviously higher for the fuel far from the gap in which less absorption is present, and therefore will tend to sharpen the flux peak in the fuel with respect to the peak in the homogenized cluster.

b) The experiments give thermal neutron reaction rates in copper rather than flux distributions. These reaction rates are given by $\bar{\sigma}\cdot\varphi$ where $\bar{\sigma}$ is an average cross section which depends on the energy distributions within φ and will be higher in the gap. In our calculations differences in energy distributions within the thermal flux are not accounted for.

This may partly explain why the calculated flux peak, with respect to the cosine distribution, is rather close to the measured reaction rate peak up to the copper foil position two centimetres from the gap, and is considerably smaller at the gap interface.

Besides that the use of diffusion theory for a rather short gap is also responsible for a flattening of the flux peak.

7. Spectrum index measurements

7.1 Scope of work

Spectrum indices were measured by foil activation techniques in two characteristic rod positions in the central fuel bundle of the test lattice, consisting of seven fuel assemblies. The techniques employed have been described in [15] and [16]. The following quantities were measured:

The indium epithermal index q/q_c, q being the ratio of the neutron density in a certain narrow energy band around the 1.46 eV indium resonance to the total neutron density. q_c is the corresponding quantity for a calibration spectrum in the R1 central channel, which is known in detail from chopper measurements. This calibration spectrum has been specified point by point e.g. in ref. [15]. It should be noted that the indium cross section does not have to be known [15]. The ratio q/q_c can easily be transformed into the Westcott index $r\sqrt{T_n}$.

The ratio $(Lu^{176}/Mn^{55})/(Lu^{176}/Mn^{55})_c$. In this case the calibration spectrum was a 25 °C Maxwellian in the R1 thermal column. The resonance correction factors for the particular manganese

foils used is well known, and hence the ratio $(Lu^{176}/1/v)/(Lu^{176}/1/v)_c$ is obtained. This ratio can be extracted directly from METHUSELAH calculations. The experimental ratio can also be used for deriving a neutron temperature T_n by means of the Westcott tables [13].

7.2 Experimental conditions

The foils were inserted between specially ground pellets with plane ends, and the resulting foil packs were placed in the middle of the openable fuel stringers. Two such stringers constituted a fuel rod. The spectrum indicator foils were protected against fission product contamination by 0.05 mm Cu foils.

The foil materials are described in Table X.

For the determination of the indium epithermal index the sandwich foil method was used. Hence the indium concentration in the foils is such as to give appreciable self-shielding at resonance energy and little self-shielding at other energies. The small thermal self-shielding that did occur was corrected for.

In the lutetium and manganese foils the thermal self-shielding could be neglected. The Mn resonance self-shielding was taken into account when correcting for resonance absorption.

7.3 Spectrum index correlations

In [16] a set of correlations was derived for the fuel-averaged spectral indices in an infinite lattice. In terms of the Westcott parameters they take the form

$$P\ r\sqrt{T_n} = 13.4 \left[\frac{V_{fuel}\ \Sigma_{fuel}}{V_m\ \Sigma_{nat}}\right]_{lattice} \tag{19}$$

$$(T_n - T_m)/T_m = 1.42 \left[\frac{V_{fuel}\ \Sigma_{fuel}}{V_m\ \Sigma_{nat}}\right]_{lattice} + 0.355\ \left[V_{fuel}\ \Sigma_{fuel}\right]_{rod} \tag{20}$$

In these expressions Σ_{fuel} is the effective thermal macroscopic absorption cross section of the fuel, i.e. Σ_{fuel}^{2200}, and $\Sigma_{nat} = 0.172\ cm^{-1}$. The factor P corrects for differential leakage in a critical lattice and can be written as

$$P = \frac{1 + 0.9\ \tau B^2}{(1 + \tau B^2)(1 + L^2 B^2)} \tag{21}$$

The volume ratios in the "lattice" terms refer to a lattice cell. The volume V_{fuel} in the "rod" term is that of a single fuel rod in the cluster, expressed in cm^3 per cm height. Table XI gives the fuel data used in the correlations.

We get $[V_{fuel}\ \Sigma_{fuel}]_{rod} = 0.553$ and $\Sigma_{fuel}/\Sigma_{nat} = 2.58$. The leakage correction factor P was calculated from values of B^2, τ and L^2 computed with METHUSELAH, where the void cases were approximated by 75 % air and 25 % D_2O.

7.4 Results

The results are presented in Table XII. In the table are also given the parameters entering the spectrum index correlations (19) and (20), as well as the results of the latter, the epithermal indices having been corrected for leakage to pertain to the critical lattices. The table further includes the r-values, computed with the diffusion code PLUTHARCO, which uses the Westcott model and has incorporated the AECL neutron temperature correlation [17]. Finally, the table gives the $(Lu/1/v)/(Lu/1/v)_c$ ratio obtained with METHUSELAH. Here only the results for the D_2O-cooled cases are given, since the METHUSELAH version used is not suited for void calculations. It is seen that for the 13 cm lattice the correlation as well as PLUTHARCO give r-values considerably higher than the experimental ones. This is undoubtably due to the fact that the test zone in this case is too small for asymptotic spectral conditions to be established. The effect should be most serious for the voided case, which agrees with the experimental tendency. Figure 20 elucidates the situation. Here the epithermal index $P\ r\sqrt{T_n}$ (which is equal to $0.720\ Pq/q_c$, see [16]) is plotted against $(V_{fuel}\ \Sigma_{fuel})/(V_m\ \Sigma_{nat})$. From the figure one may deduce a correction factor of roughly 1.2 for the unvoided and 1.4 for the voided 13 cm lattice to compensate for non-asymptotic conditions. Approx-

imately the same factors should apply to (RCR_∞ - 1). The r-values of the correlations and PLUTHARCO agree within 6 %. The measured neutron temperature is consistently lower than that of the correlations. This conforms with earlier findings that the correlations tend to overestimate T_n for high fuel concentrations (high enrichment or large rod diameters). The agreement between METHUSELAH calculations and experimental values of the lutetium reaction rate ratios is within about 2 %, which must be considered satisfactory.

8. Conversion ratio measurements

8.1 Scope of work

The main purpose of the experiment was to gain experience and confidence with the methods used since the initial conversion ratio had later on to be measured in HBWR.

The studies in RO were made in the 13 and 17 cm lattices and the coolant was either D_2O or air.

The initial conversion ratio γ_o is the number of fissile atoms produced per fissile atom destroyed in fresh fuel. For the fuel under consideration the fast fission of Th^{232} [18] and U^{238} and the production of Pu^{239} in U^{238} are negligible. Neutron capture in Th^{232} results in the following decay chain

$$Th^{232} + n \longrightarrow Th^{233} \xrightarrow[23\ min]{\beta^-} Pa^{233} \xrightarrow[27.4\ d]{\beta^-} U^{233} \qquad (22)$$

Consequently only the number of U^{233} atoms (fissile) produced and the number of U^{235} atoms destroyed have to be considered.

It is, however, hard to determine the total number of U^{235} atoms destroyed with high accuracy. More readily we can get a quantity proportional to the number of those U^{235} atoms which are destroyed by fission. Further, it is advantageous to measure relative to the conditions in a thermal spectrum. The quantity that we get experimentally in this way is called the "modified relative conversion ratio" (RCR^x) and is defined as

$$RCR^x = \frac{(Th^{232}\ \text{capture rate})_{lattice}}{(Th^{232}\ \text{capture rate})_{thermal}} \times \frac{(U^{235}\ \text{fission rate})_{thermal}}{(U^{235}\ \text{fission rate})_{lattice}} \qquad (23)$$

or

$$RCR^{*} = \frac{(Pa^{233}\ \text{activity})_{lattice}}{(Pa^{233}\ \text{activity})_{thermal}} \times \frac{(U^{235}\ \text{FP act.})_{thermal}}{(U^{235}\ \text{FP act.})_{lattice}} \qquad (24)$$

where FP = fission product.

The word "modified" is used because the U^{235} captures are excluded.

RCR^{*} according to eq. (24) is related to γ_o as follows

$$\gamma_o = RCR^{*} \left[\frac{\Sigma_a(Th^{233})}{\Sigma_a(U^{235})}\right]_{thermal} \times \left[\frac{(1+\bar{\alpha})_{thermal}}{(1+\bar{\alpha})_{lattice}}\right] \qquad (25)$$

where $\bar{\alpha}$ is the ratio of capture-to-fission cross sections of U^{235} averaged over the spectrum as follows

$$\bar{\alpha} = \int \alpha\phi\Sigma_f dE \ / \int \phi\Sigma_f dE = \bar{\Sigma}_c/\bar{\Sigma}_f \qquad (26)$$

8.2 Experimental technique

Fuel discs of 0.3 mm med 3.0 mm thickness were irradiated simultaneously in the test lattice of R0 and in the thermal column of R2-0. The irradiation time was 4 hours and the thermal neutron flux was about 2×10^8 n/cm^{2}sec.

In the fuel assembly the 0.3 and 3.0 mm discs were placed at some distances from the fuel gap, viz. 16 cm and 24 cm respectively. The 0.3 mm wafers had to be carefully aligned. Therefore one wafer and two adjacent fuel pellets were put together in a fuel pack by means of adhesive tape. The sample in the thermal column was a small pack containing discs of the following thicknesses: 1.5 + 0.3 + 0.3 + 3.0 + 1.5 (= 6.6)mm. The 3 mm fuel pellets were dissolved chemically prior to counting, in order to produce samples with homogeneous activity distribution. The 0.3 mm wafers were, however, not dissolved but counted directly.

The Pa^{233} γ-activity was measured in a window from 270 to 370 keV. Simultaneously the fission product γ-activity was measured above a discriminator level of 510 keV, where no contamination from the Pa^{233} activity

was observed. However, besides the Pa^{233} γ-activity there appears in the window also some γ-activity coming mainly from U^{235} fission products. Thus we had to correct for this background activity which was possible by measuring in the same energy intervals on an enriched uranium sample with 93 % U^{235} irradiated simultaneously with the fuel samples in RO.

For comparative reasons we tried two types of enriched uranium samples, viz. a powder sample of uranium oxide, weight about 40 mg, and a 0.1 mg deposit of uranium on an aluminium disc. The powder was dissolved afterwards. In this way we got a sample with the same geometry as that of the other liquid samples. The 0.1 mg deposit needed of course a comparatively high neutron flux in order to become sufficiently activated, but otherwise we could not discover any difference between the two samples.

The corrected Pa^{233} activity in the window can now be evaluated from the following expression:

$$Pa^{233}\ \text{activity} = A_{fu}(270\text{-}370) - A_{fu}(>510) \cdot \frac{A_e(270\text{-}370)}{A_e(>510)} \qquad (27)$$

where

A_i is the measured activity of sample i (corrected for background activity),

fu and e (subscripts) refer to fuel and enriched uranium respectively,

>510 means above 510 keV, and

270-370 stands for from 270 keV - 370 keV .

The countings in the window (270-370 keV) and above 510 keV were made simultaneously for each sample. The time dependence is consequently of little importance in eq. (27), since the ratio A(270-370)/A(>510) is to a good approximation constant during the time periods of interest here.

Otherwise the samples were counted in a back-and-forth sequence (1, 2, 3, ..., n-1, n; n, n-1, ..., 3, 2, 1). The counting intervals were 300 or 1000 sec. and an interval of 15 sec. allowed for sample changing and tape punching. The fission product decay curve was linearized

within each cycle, so that the average of the two countings of each foil was considered as related to the same time for all foils. Owing to the long counting intervals this assumption is not exact, but the maximum error introduced in the ratio of FP activity in eq. (24) was less than $2 \cdot 10^{-4}$ [12].

In order to investigate whether the spectrum in the thermal column of R2-0 was affected significantly by the sample itself (thickness 6.6 mm) an auxiliary experiment was carried out. Four packs of fuel pellets, 0.9, 3.3, 6.3, and 9.3 mm thick respectively and arranged as shown in fig. 21, were simultaneously irradiated on a rotating graphite cylinder in the thermal column of R2-0. The RCR* (relative to a fixed reference foil) for the 0.3 mm thick inner foil of each pack was determined. The results plotted in fig. 22 show that the contribution of induced epithermal neutrons is insignificant within the experimental error of $\pm$ 0.5 %.

The counting data were treated with the computer programs KODAFIP (fission product activity) [19] and KODAK (Pa^{233} activity) [20].

8.3 Results

The measured values were obtained from countings taken at different times (from 1 day to 80 days approximately) after the end of the irradiation. Only the most reliable values are reported here (see Table XIII). The other values were rejected for at least one of the following reasons:

- Too low activity above background
- Unknown background
- Too large FP correction (too short time after irradiation)
- Too high count rate causing fatigue effects in the photomultiplier tube
- Leakage from one of the teflon containers.

The errors given in Table XIII are random errors.

Fig. 23 shows the measured FP correction and the natural background activity of the Pa samples as a function of time after irradiation. Countings taken more than 4 days and less than 20 days after irradiation were considered in the analysis of the measurements.

The minimum fission product correction was in our case about 10 % (cf. fig. 23). The natural background activity in the Pa window (270-370 keV) was relatively high due to the low integrated power. Unfortunately background samples were not included in the counting cycles except in the case of liquid samples from the irradiations in the 13 cm lattice with D_2O as coolant.

In fig. 24 (RCR^*-1) values have been plotted as a function of $(V_{fuel}\ \Sigma_{fuel})/(V_m\ \Sigma_{nat})$, i.e. the same variable as used for spectral indices (cf. section 7).

The calculated values of RCR^* were obtained with METHUSELAH and were corrected for leakage. The values referring to voided channels have been obtained by linear extrapolation of the values calculated for zero and 50 % void, since METHUSELAH is unable to treat 100 % void. The extrapolated values are uncertain. According to the results of epithermal indices (cf. fig. 20) we cannot neglect the influence of non-asymptotic spectral conditions, at least not in the 13 cm lattice. The experimental and theoretical values of RCR^* shown in fig. 24 are consequently not directly comparable for the most interesting case, i.e. the 13 cm lattice.

8.4 Recommendations for future measurements

A better accuracy can be obtained with the methods used taking the following recommendations into consideration:

- The integrated power should be at least a factor 2 larger than the one used in RO in order to get a Pa^{233} activity well above background.
- If the enriched sample used for FP correction is placed in the lattice position, it should contain a sufficient amount of U^{235} to give proper counting statistics.
- Fission product correction samples should always be counted along with the other samples.
- Two background samples (unirradiated $ThO_2/U^{235}O_2$ and unirradiated 93 % enriched samples) should be placed in the foil stack.

- The total count rate above 100 keV should not exceed 1000 counts/sec. in order to avoid fatigue effects in the photomultiplier tube.

9. Conclusions

With only seven $ThO_2/U^{235}O_2$ fuel assemblies available the progressive substitution technique had to be applied for buckling measurements. Since the pitches of the test and reference lattices were the same, we believe that there are no essential difficulties in the analysis with $ThO_2/U^{235}O_2$ as test fuel. Assuming reference bucklings to be exact we determine buckling differences between $-3.5\ m^{-2}$ and $+1.5\ m^{-2}$ with an estimated accuracy better than $0.1\ m^{-2}$. However, the 11 cm (or more precisely $19/\sqrt{3}$ cm) reference lattice consisted of only 36 metal rods and was obtained by adding 24 metal rods in the central part of an approximately full-core 19 cm lattice. Due to the very different pitches in the two regions in this case and the corresponding great spectral mismatch (though approximately equal bucklings) we find that the analysis is not quite straightforward but involves problems in the definition of the transition region. The number of regions involved should not be critical, since the computer program SIMBA is able to handle up to 8 regions.

Systematic buckling errors due to quality differences between $ThO_2/U^{235}O_2$ fuel assemblies were found to be significant, especially for the larger pitches. The special fuel assembly used for activation experiments was 10-30 pcm more reactive than the other assemblies.

Flux peaking at the fuel gap caused a maximum increase of 40-50 % in the power distribution close to the gap. Diffusion theory calculations with EQUIPOISE underestimate the peaking considerably.

Spectral studies showed that non-asymptotic epithermal-spectrum conditions prevailed in the test zone with the lattice pitch (13 cm) equal to that of HBWR. Activity ratios of Lu/Mn, which may be interpreted in terms of"neutron temperature", showed good agreement with METHUSELAH calculations also for the tight lattice.

The conversion ratio measurements were not altogether successful but gave valuable experience for similar experiments in HBWR in September 1967.

10. Acknowledgements

We are much obliged to the operations group at RO for a very careful and efficient work. We especially wish to express our thanks to E. Wendler and J. Gjödestöl for their quick response on changes desired during the experimental period. The skilful technical assistance by R. Bladh in the activation experiments is much appreciated and our thanks are also due to C-E. Wikdahl for helpful discussions.

References

1. R. Alpiar
METHUSELAH I. A universal assessment programme for liquid moderated reactor cells, using IBM-7090 or STRETCH computers
AEEW-R 135 (1964)

2. W. De Haan and R. Meelhuysen
PLUTHARCO, a PLutonium, Uranium THorium Assembly Reactivity COde. Physical concept, comparison with experiments and code description
EUR 3141.e (1966)

3. P.-E. Ahlström and B. Eriksson
REBUS. A recipe for calculation of lattice parameters and burnup in heavy water moderated reactors
AE-RFR-542, -550, -560 (1966)

4. T.B. Fowler and M.L. Tobias
EQUIPOISE 3: A two-dimensional, two-group, neutron diffusion code for the IBM-7090 computer.
ORNL-3199 (1962)

5. P. Benoist
Théorie du coefficient de diffusion des neutrons dans un réseau comportant des cavités
CEA-R 2278 (1964)

6. R. Persson
Perturbation method of analysis applied to substitution measurements of buckling
AE-256 (1966)

7. R. Persson
One-group perturbation theory applied to measurements with void
AE-248 (1966)

8. R. Lindh and R. Persson
SIMBA, Simple Iterative Method of Buckling Analysis. Computer program and formulas
AE-TPM-FFR-90 (1967)

9. S. Grifoni
Program CRACOB
AE-TPM-FFR-86 (1967)

10. R. Persson
Semi-empirical formula for the change of diffusion coefficients caused by empty channels
Reactor Sci. Techn. (J. Nucl. Energy Parts A/B) 20, 671 (1966)

11. P.-E. Ahlström
Private information

12. C.B. Bigham and P.R. Tunnicliffe
Experimental effective fission cross section and neutron spectra in a uranium fuel rod
AECL-1186 (1961)

13. C.H. Westcott
Effective cross-section values for well-moderated thermal reactor spectra
AECL-1101 (1962)

14. D.A. Newmarch
RIPPLE. A method of computing thermal neutron fine structure of thin plate assemblies
AERE R/R 2425 (1959)

15. E. K. Sokolowski
J. Nucl. Energy 21, 35 (1967)

16. E.K. Sokolowski and A. Jonsson
Epithermal and thermal spectrum indices in heavy-water lattices
AE-277 (1967)

17. B.G. Chidley, R.P. Turner, and C.B. Bigham
Experimental effective fission cross-sections and neutron spectra in a uranium fuel rod. Part 2. CANDU-type fuel with H_2O-D_2O mixture as coolant
AECL-1419 (1961)

18. J. Weitman
The effective resonance integral of thorium oxide rods
AE-99 (1962)

19. Å. Ahlin and H. Pekarek
KODAFIP, a computer program for the evaluation of fission product activity data
AE-TPM-FFR-53 (1965)

20. Å. Ahlin, H. Pekarek and L.I. Tirén
KODAK, a computer program for the evaluation of Np^{239} activation data
AE-FFR-3 (1964)

Table I

Critical heights in the substitution measurements with U metal rods.

Reference pitch: 19 cm

Test pitch : $19/\sqrt{3}$ cm

Subst. step	$H_{exp.}$ [mm]	Temp. [°C]	$\partial\rho/\partial H$ [pcm/mm]	$H_{corr.}$ * (22 °C) [mm]
Pure reference	1936.9	22.13	6.8	2036.4
Ref. with spikes (Fig. 7)	1760.6	22.19	9.0	1860.1
Fig. 4a	1741.3	22.28	8.6	1840.4
Fig. 4b	1731.5	22.26	8.4	1830.6
Fig. 4c	1714.8	22.28	8.7	1813.9
Fig. 4d	1689.8	22.23	8.4	1788.9
Fig. 4e	1689.9	22.40	8.4	1788.5

Buckling of the reference lattice: 6.77 m^{-2}

" " " test " : 6.76 ± 0.02 m^{-2}

*) $H_{corr.}$ is obtained from $H_{exp.}$ (level meter) by adding 100 mm due to scale adjustment and extrapolation lengths and by correcting for temperature variations by $\delta T(\partial\rho/\partial T):(\partial\rho/\partial H)$ with $\partial\rho/\partial T = 25$ pcm/°C.

Table II

Critical heights in the single-element measurements of $\delta D_z/D$
Pitch: 17 cm

Void depth [mm]	$H_{exp.}$ [mm]	Temp. [°C]	$\partial\rho/\partial H$ [pcm/mm]	$H_{corr.}$ * (22 °C) [mm]
394.1	1668.2	22.39	9.2	1767.4
606.2	1667.6	22.39	9.2	1766.8
815.7	1667.3	22.39	9.2	1766.5
1006.6	1666.7	22.39	9.2	1765.9
1216.9	1666.1	22.39	9.2	1765.3
1381.9	1665.4	22.39	9.3	1764.6
1518.9	1664.7	22.39	9.3	1763.9
1664.1	1664.1	22.39	9.3	1763.3

* See Table I

A graphical evaluation of the measurements is given in fig. 6.

Table III

Critical heights in the single-element measurements of $\delta D_r/D$.
Pitch: 17 cm

Radial position [mm]	Coolant [W = D_2O A = air]	$H_{exp.}$ [mm]	Temp. [°C]	$\partial\rho/\partial H$ [pcm/mm]	$H_{corr.}$ * (22 °C) [mm]
0/0	W	1664.6	22.46	9.3	1763.6
	A	1670.5	22.46	9.2	1769.2
170/0	W	1666.6	22.55	9.2	1765.1
	A	1672.2	22.55	9.2	1770.7
340/0	W	1667.9	22.66	9.2	1766.1
	A	1673.0	22.66	9.2	1771.2
510/0	W	1670.3	22.67	9.2	1768.5
	A	1673.8	22.67	9.2	1772.0
510/0	W	1668.3	22.61	9.2	1766.6
	A	1672.4	22.61	9.2	1770.7
680/0	W	1671.3	22.75	9.2	1769.3
	A	1674.3	22.74	9.2	1772.3
850/0	W	1673.1	22.84	9.2	1770.8
	A	1675.3	22.83	9.2	1773.0

* See Table I

A graphical evaluation of the measurements is given in fig. 7.

Table IV

Intercomparison of ThO_2 fuel assemblies in the 13 cm reference lattice

Fuel assembly notation	$H_{exp.}$ [mm]	Temp. [°C]	$\partial\rho/\partial H$ exp. [pcm/mm]	$H_{corr.}$ * (20.5 °C) [mm]	Mean density of fuel [g/cm³]	$U^{235}O_2$ [w/o]
A	1619.5	20.39	8.3	1719.8	9.58	1.998
B	1619.8	20.61	(8.2)	1719.5	9.57	1.991
C	1620.1	20.51	8.2	1720.1	9.57	1.995
D	1619.8	20.49	8.4	1719.8	9.59	1.995
E	1620.4	20.55	(8.1)	1720.2	9.55	1.993
F	1620.0	20.40	7.9	1720.3	9.51	1.996
G**	1618.9	20.64	(8.5)	1718.5	9.61	2.016
Mean values of all assemblies				1719.74	9.568	1.998
Mean values with G excluded				1719.95	9.562	1.995

* See Table I

** G is the special fuel assembly used in connection with activation experiments.

Table V

Critical heights in the substitution measurements with ThO_2 fuel assemblies. Pitches: $19/\sqrt{3}$ (≈ 11.0) cm and 13 cm

Pitch [mm]	Subst. step	Coolant	$H_{exp.}$ [mm]	Temp. [°C]	$\partial\rho/\partial H$ [pcm/mm]	$H_{corr.}$* (22 °C) [mm]
$190/\sqrt{3}$	Ref.	-	1689.9	22.40	8.4	1788.5
	1	D_2O	1686.7	22.42	8.5	1785.2
	2	"	1682.9	22.53	8.6	1781.1
	3	"	1680.0	22.63	8.6	1778.0
	4	"	1676.4	22.71	8.7	1774.1
	5	"	1672.9	22.79	8.8	1770.4
	7	"	1665.4	22.75	8.9	1763.0
	1	Air	1699.2	22.42	8.2	1797.8
	2	"	1707.3	22.52	8.0	1805.7
	3	"	1716.2	22.62	7.8	1814.3
	4	"	1724.6	22.71	7.7	1822.5
	5	"	1733.4	22.75	7.5	1831.2
	7	"	1750.8	22.75	7.1	1848.7
130	Ref. with driver	-	1527.5	20.80	9.7	1630.0
	1	D_2O	1523.6	20.82	9.8	1626.1
	2	"	1519.9	20.94	9.9	1622.0
	3	"	1516.8	21.05	10.0	1618.6
	4	"	1513.0	21.16	10.1	1614.5
	5	"	1509.3	21.26	10.2	1610.6
	5**	"	1509.3	21.36	10.2	1610.3
	7	"	1501.2	21.47	10.5	1601.9
	7***	"	1708.7	21.54	7.4	1810.6
	1	Air	1532.0	20.82	9.6	1634.7
	2	"	1536.8	20.94	9.5	1639.3
	3	"	1542.3	21.04	9.4	1644.7
	4	"	1547.2	21.16	9.3	1649.4
	5	"	1551.7	21.25	9.2	1653.8
	5**	"	1551.6	21.35	9.2	1653.4
	7	"	1560.5	21.44	9.1	1662.3

* See Table I.

** Cf. fig. of

Table VI

Critical heights in the substitution measurements with ThO_2 fuel assemblies
Pitches: 15 cm and 17 cm

Pitch [mm]	Subst. step	Coolant	$H_{exp.}$ [mm]	Temp. [°C]	$\partial\rho/\partial H$ [pcm/mm]	$H_{corr.}$* (22 °C) [mm]
150	Ref.	-	1574.1	21.79	9.3	1674.2
	1	D_2O	1567.7	21.77	9.4	1667.9
	2	"	1560.5	21.69	9.5	1660.9
	3	"	1556.8	22.27	9.6	1655.7
	4	"	1551.7	22.13	9.6	1650.9
	5	"	1545.0	22.02	9.8	1644.5
	5**	"	1544.8	21.90	9.8	1644.6
	7	"	1530.8	21.75	10.0	1631.0
	1	Air	1575.1	21.77	9.2	1675.4
	2	"	1575.1	21.68	9.2	1675.8
	3	"	1578.8	22.27	9.2	1678.0
	4	"	1581.5	22.12	9.1	1681.2
	5	"	1581.7	22.01	9.1	1681.8
	5**	"	1581.1	21.90	9.1	1681.5
	7	"	1582.3	21.71	9.1	1683.5
170	Ref.	-	1669.7	21.80	8.9	1769.9
	1	D_2O	1660.5	21.80	9.0	1760.7
	2	"	1652.5	21.93	9.2	1752.4
	3	"	1645.5	21.98	9.3	1745.2
	4	"	1636.5	22.09	9.4	1735.9
	5	"	1630.3	22.18	9.5	1729.5
	7	"	1612.1	22.32	9.8	1710.9
	1	Air	1666.5	21.80	9.0	1766.8
	2	"	1664.1	21.93	9.0	1764.2
	3	"	1663.3	21.98	9.0	1763.3
	4	"	1660.6	22.09	9.0	1760.5
	5	"	1660.0	22.17	9.1	1759.7
	7	"	1654.4	22.32	9.1	1754.0

* See Table I

** Cf. fig. 9f

Table VII

Summary of experimental material bucklings

Temperature: 22 °C

Moderator quality: 99.645 w/o D_2O

Hexagonal lattice pitch [cm]	B^2_{ref} [m^{-2}]	Type[x] of analysis	B^2_{test} Coolant: D_2O [m^{-2}]	B^2_{test} Coolant: air [m^{-2}]	$B^2(D_2O)-B^2(air)$ [m^{-2}]
11	6.76	Ia	8.36 ± 0.04		
		Ib	8.31 ± 0.04	3.22 ± 0.07	5.09
		IIa	8.31 ± 0.07		
		IIb	8.22 ± 0.07	3.07 ± 0.06	5.15
13	8.32	Ia	9.87 ± 0.06		
		Ib	9.78 ± 0.06	5.87 ± 0.07	3.91
		IIa	9.89 ± 0.08		
		IIb	9.76 ± 0.07	5.87 ± 0.11	3.89
15	8.23	Ia	9.83 ± 0.13		
		Ib	9.70 ± 0.08	6.80 ± 0.09	
		Ib[xx]	9.69 ± 0.03	6.78 ± 0.02	2.91
		IIa	9.91 ± 0.16		
		IIb	9.72 ± 0.11	6.79 ± 0.15	
		IIb[xx]	9.71 ± 0.04	6.77 ± 0.03	2.94
17	7.61	Ia	9.14 ± 0.09		
		Ib	9.03 ± 0.05	7.19 ± 0.03	1.84
		IIa	9.26 ± 0.14		
		IIb	9.09 ± 0.07	7.22 ± 0.06	1.87

x) Ia: One transition region, no fuel quality correction

Ib: " " " , fuel quality correction applied (H = 1719.95 mm in Table IV)

IIa: Two transition regions, no fuel quality correction

IIb: " " " , fuel quality correction applied (H = 1719.95 mm in Table IV)

xx) Substitution with 4 test fuel assemblies omitted

Table VIII

Flux peaking at the fuel gap

Axial position	Inner stringer		Outer stringer	
	Coolant		Coolant	
	D_2O	Air	D_2O	Air
Upper end of gap	1.52	1.43	1.43	1.38
Lower end of gap	1.55	1.45	1.46	1.42

Table IX

Calculated correction in B^2 due to the gap

Pitch [cm]		11	13	15	17
k_{eff} with gap			1.09763		1.12987
k_{eff} without gap			1.09781		1.13155
δB^2 $[m^{-2}]$	D_2O	(-0.01)	0.011	(0.04)	0.074
	air	(-0.03)	(-0.01)	(0.02)	(0.05)

Table X

Foil materials used in spectrum index measurements

Foil composition	Thickness [mm]	Diam. [mm]
In 2.5 w/o Pb 97.5 w/o	0.10	12.0
Lu 7.2 w/o Al 92.8 w/o	0.15	12.0
Mn 12 w/o Ni 88 w/o	0.127	12.0

Table XI

Fuel data used in spectrum index correlations

Nuclide i	Number density [cm^{-3}]	σ^{2200} [b]	g(Westcott)	Σ_i [cm^{-1}]
Th^{232}	2.14×10^{22}	7.56	1.00	0.162
U^{235}	4.33×10^{20}	679.9	0.96	0.282
U^{238}	4.71×10^{19}	2.71	1.00	negl.

$\Sigma_{fuel} = 0.444\ cm^{-1}$

Table XII

Triangular pitch [cm]	Coolant	$\frac{V_{fuel}\Sigma_{fuel}}{V_m\Sigma_{nat}}$	Leakage factor P	Stringer*	q/q_c	$(Lu/l/v)/(Lu/l/v)_c$ meas.	$(Lu/l/v)/(Lu/l/v)_c$ METHUSELAH	r meas.	r correl. (19) and (20)	r PLUTHARCO	T_n (°C) meas.	T_n (°C) correl. (19) and (20)
13.0	D_2O	0.168	0.928	1A	3.10±.25	1.47±.02						
				1B	3.33±.27	1.41±.02						
				2A	2.77±.22	1.38±.02						
				2B	2.68±.21	1.35±.02						
				Vol.weighted fuel average	2.80±.16	1.38±.02	1.41	0.100±.006	0.118	0.113	130±7	147
	Air	0.215	0.941	1A	3.31±.27	1.39±.02						
				1B	4.00±.32	1.46±.02						
				2A	2.75±.22	1.37±.02						
				2B	2.92±.23	1.34±.02						
				Vol.weighted fuel average	2.96±.17	1.37±.02		0.106±.006	0.145	0.137	128±6	167
17.0	D_2O	0.0947	0.898	1A	2.10±.17	1.31±.01						
				1B	2.11±.17	1.31±.01						
				2A	1.68±.13	1.26±.01						
				2B	1.60±.13	1.26±.01						
				Vol.weighted fuel average	1.71±.10	1.27±.01	1.24	0.065±.004	0.072	0.071	91±5	117
	Air	0.108	0.905	1A	2.55±.20	1.35±.02						
				1B	2.42±.19	1.28±.01						
				2A	2.15±.17	1.26±.01						
				2B	2.04±.14	-						
				Vol.weighted fuel average	2.15±.10	1.27±.02		0.081±.005	0.080	0.079	89±9	122

* "1" and "2" indicate inner and outer rods, "A" and "B" upper and lower stringer, respectively

Table XIII

Lattice pitch [cm]	Coolant	$\frac{V_{fuel}\ \Sigma_{fuel}}{V_m\ \Sigma_{nat}}$	Stringer No.	RCR* Liquid samples a) (15-19 days after irradiation)	RCR* 0.3 mm foils a) (4-5 days after irradiation)	RCR* METHUSELAH (extrapolated in the air case)
13	D_2O	0.168	1	1.38 ± 2 %	1.275 ± 1 %	1.25
			2	1.47 ± 2 %	1.295 ± 1 %	
			3	1.42 ± 4 %	1.275 ± 1 %	
			4	1.35 ± 2 %	1.255 ± 1 %	
			average	1.39 ± 4 %	1.265 ± 1 %	
	Air	0.215	1	-	1.27 ± 4 %	(1.27)
			2	1.19 ± 1 %	1.29 ± 4 %	
			3	1.13 ± 1 %	1.27 ± 4 %	
			4	1.15 ± 1 %	1.28 ± 4 %	
			average	1.15 ± 1 %	1.28 ± 4 %	
17	D_2O	0.095	1	1.08 ± 1 %		1.15
			2	1.14 ± 1 %		
			3	1.14 ± 1 %		
			4	1.13 ± 1 %		
			average	1.13 ± 1 %		
	Air	0.103	1	1.18 ± 2 %		(1.13)
			2	1.17 ± 1 %		
			3	1.11 ± 1 %		
			4	1.11 ± 1 %		
			average	1.12 ± 2 %		

a) Experimental values are not corrected for non-asymptotic spectral conditions

	Cross section of fuel assembly and sketch of axial position of the ThO_2 fuel assembly in the RO tank.	FTR-113 Fig. 1

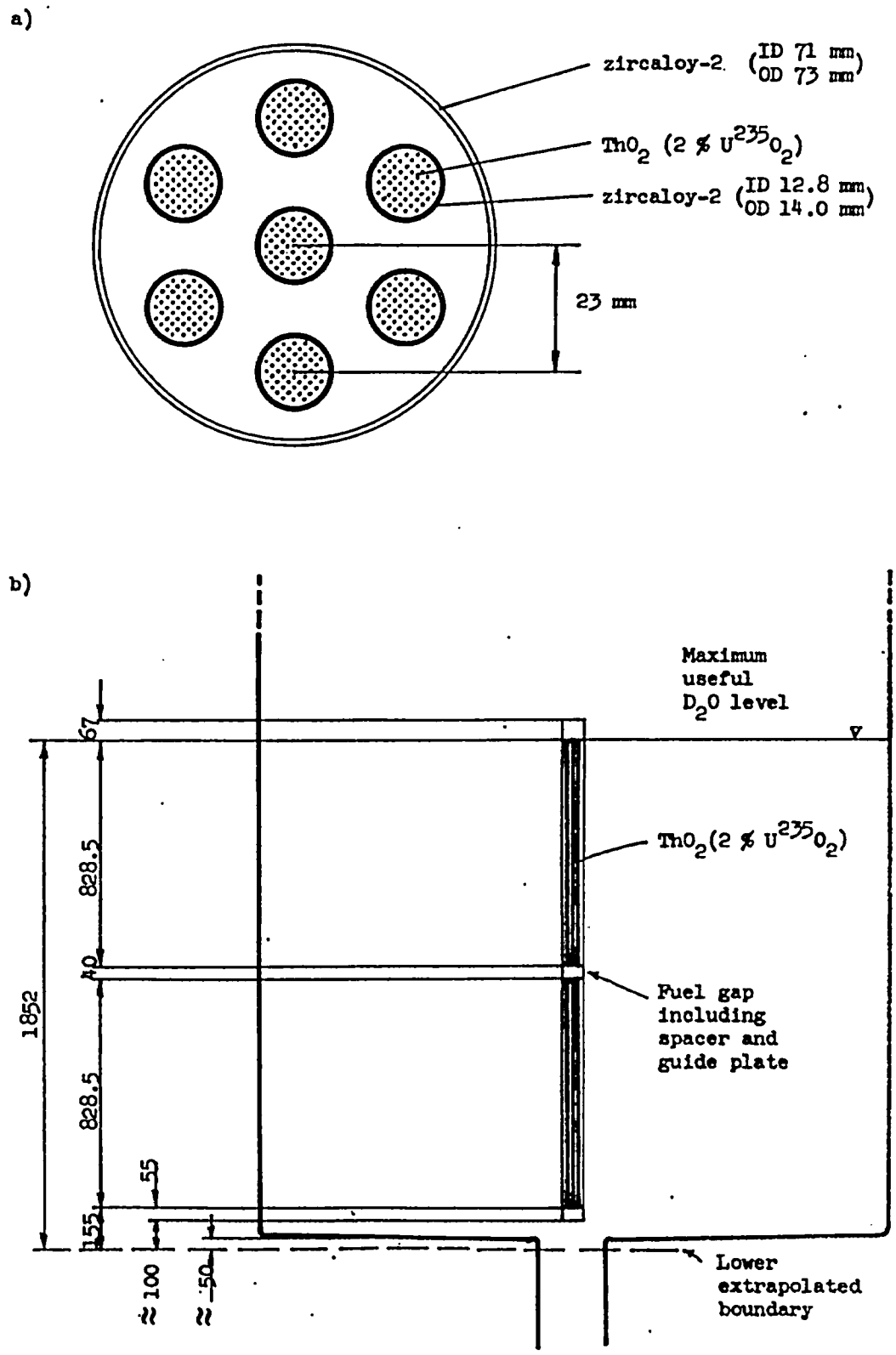

ESSELTE 4401

	Core arrangement for the $19/\sqrt{3}$ (≈ 11) cm test lattice of ThO_2 fuel assemblies.	FFR-113 Fig. 2

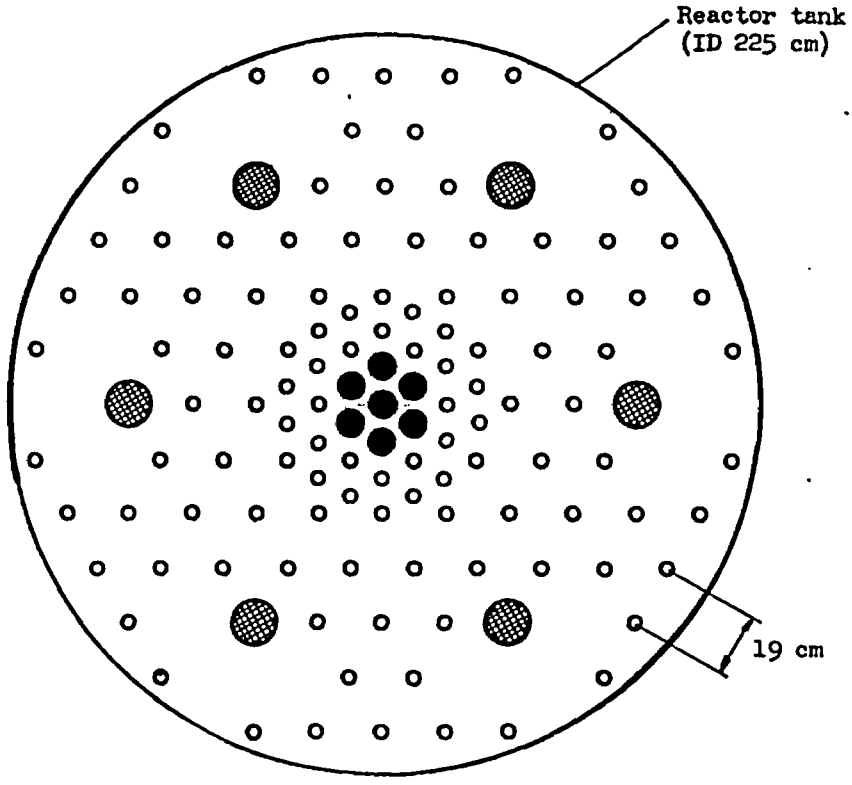

o reference rod (U metal)

● ThO_2 fuel assembly

31-rod cluster of UO_2 (1.2 % U-235)

ESSELTE
4401

	Core arrangement for the 13 cm test lattice of ThO_2 fuel assemblies.	FFR-173 Fig. 3

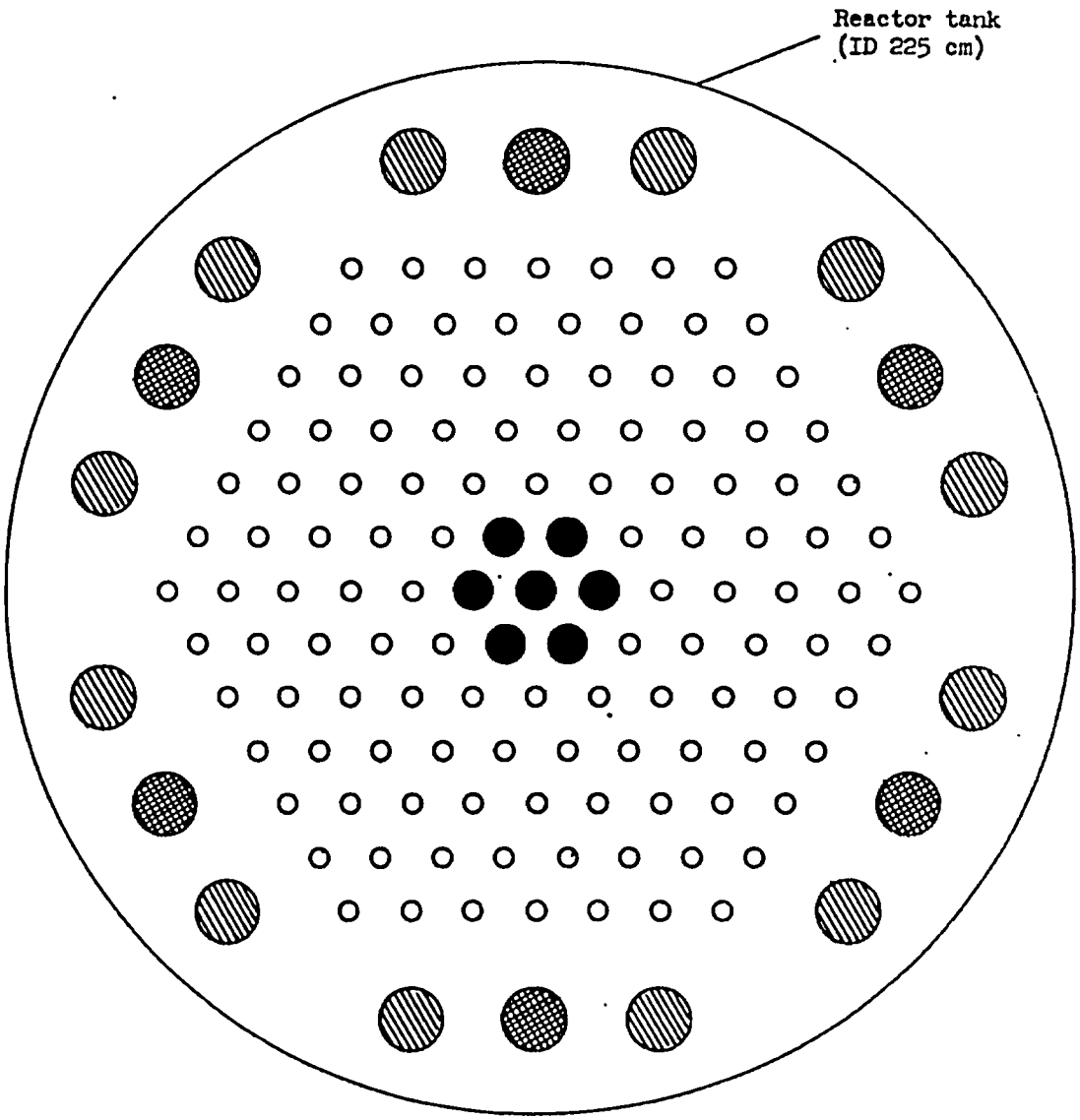

reference rod (U-metal)

ThO_2 fuel assembly

31-rod cluster of UO_2 (1.2 % U-235)

27-rod cluster of UO_2(nat.)

723501-113 A4
ESSELTE
4401

	Cell definitions used for substitutions with the $19/\sqrt{3}$ cm test pitch in a 19 cm reference lattice.	FFR-113 Fig. 4

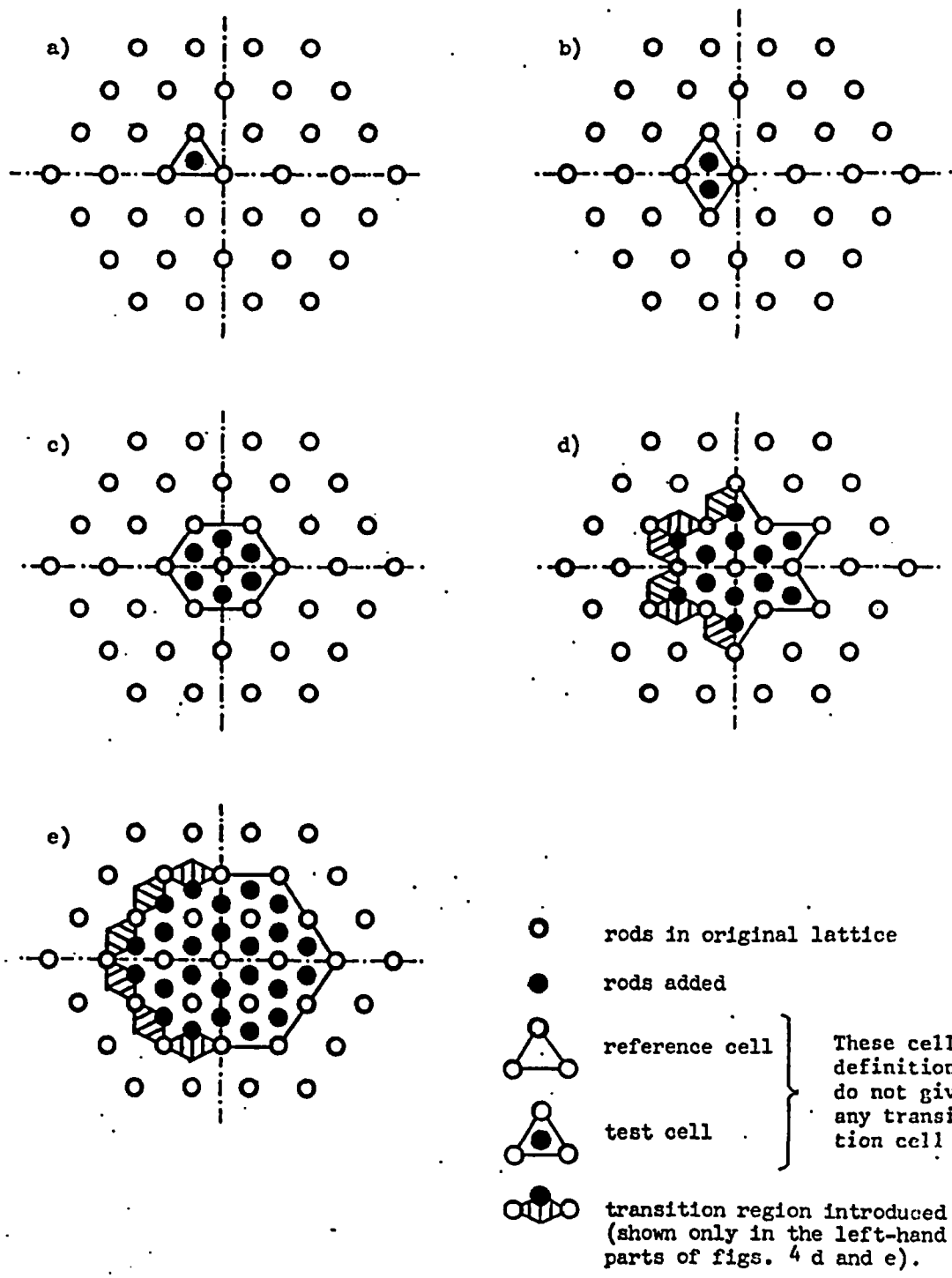

	Transition cell radii used in the 19-to-19/$\sqrt{3}$/cm substitutions of reference rods. Goodness of the fitted heights (see insert)	FFR-113 Fig. 5

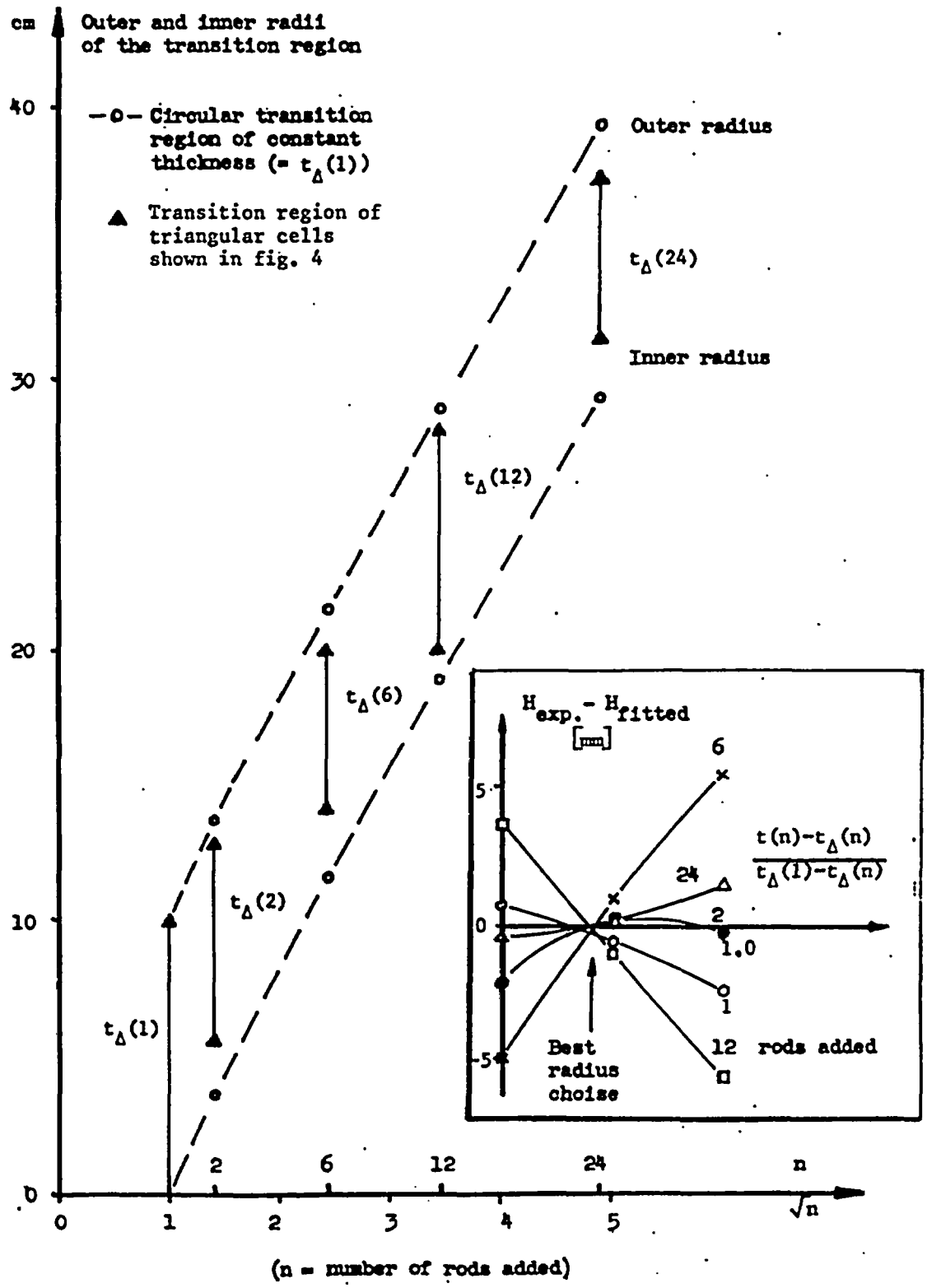

	The change in critical height versus the void depth in a single ThO_2 element. Determination of $\delta D_z/D$.	FFR-113 Fig. 6

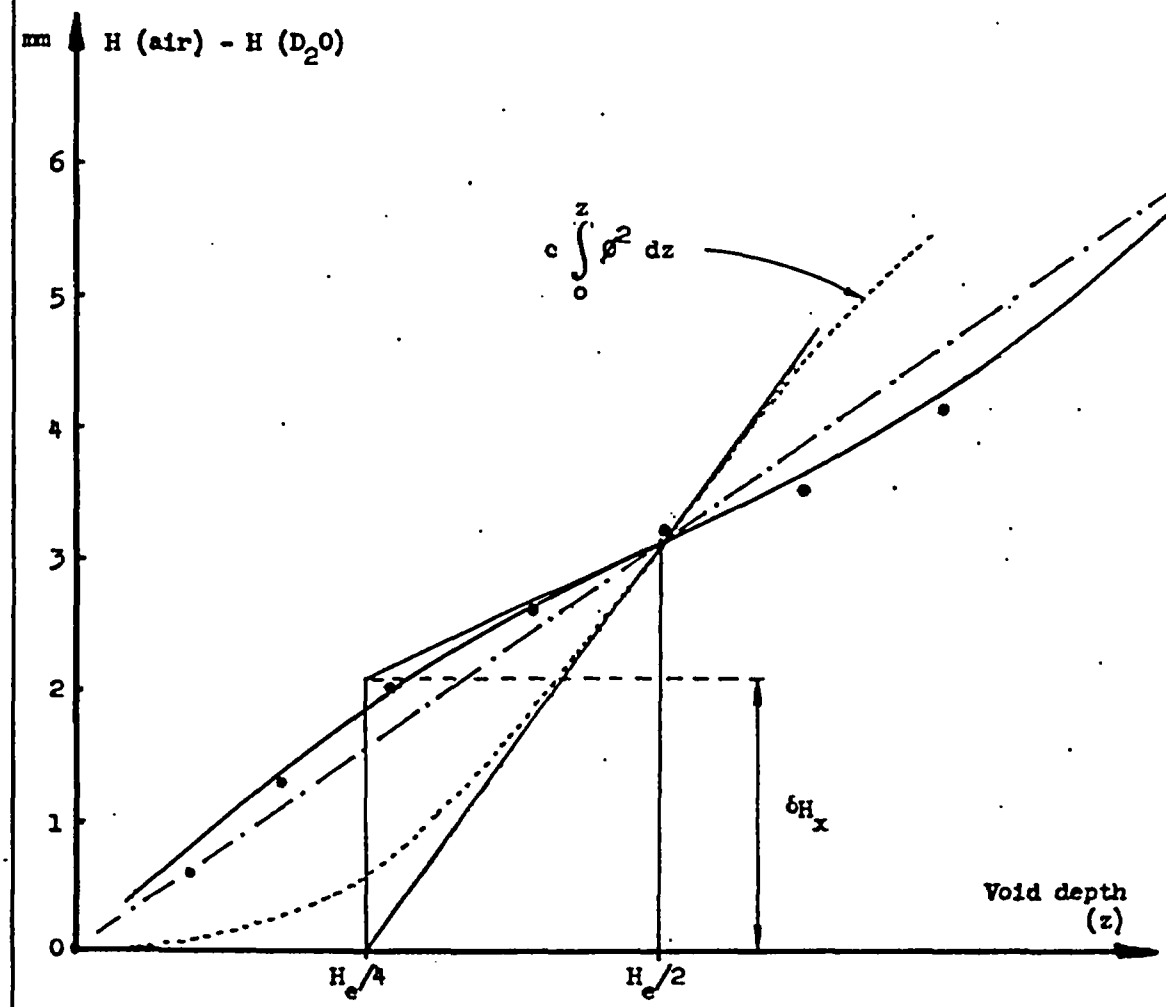

$$\frac{\delta D_z}{D} V_{cell} = 4 \frac{\delta H_x}{H_e} \cdot \frac{V_{cell}}{W_r}$$

$$= 4 \frac{2.08}{1764} \cdot \frac{17^2 \cdot \sqrt{3}}{2 \cdot 0.0218}$$

$$= 54.2 \ (\pm 3) \ cm^2$$

ESSELTE 4401

	The evaluation of $\delta D_r/D$ from substitution measurements with a single ThO_2 element in various radial positions.	FFR-113 Fig. 7

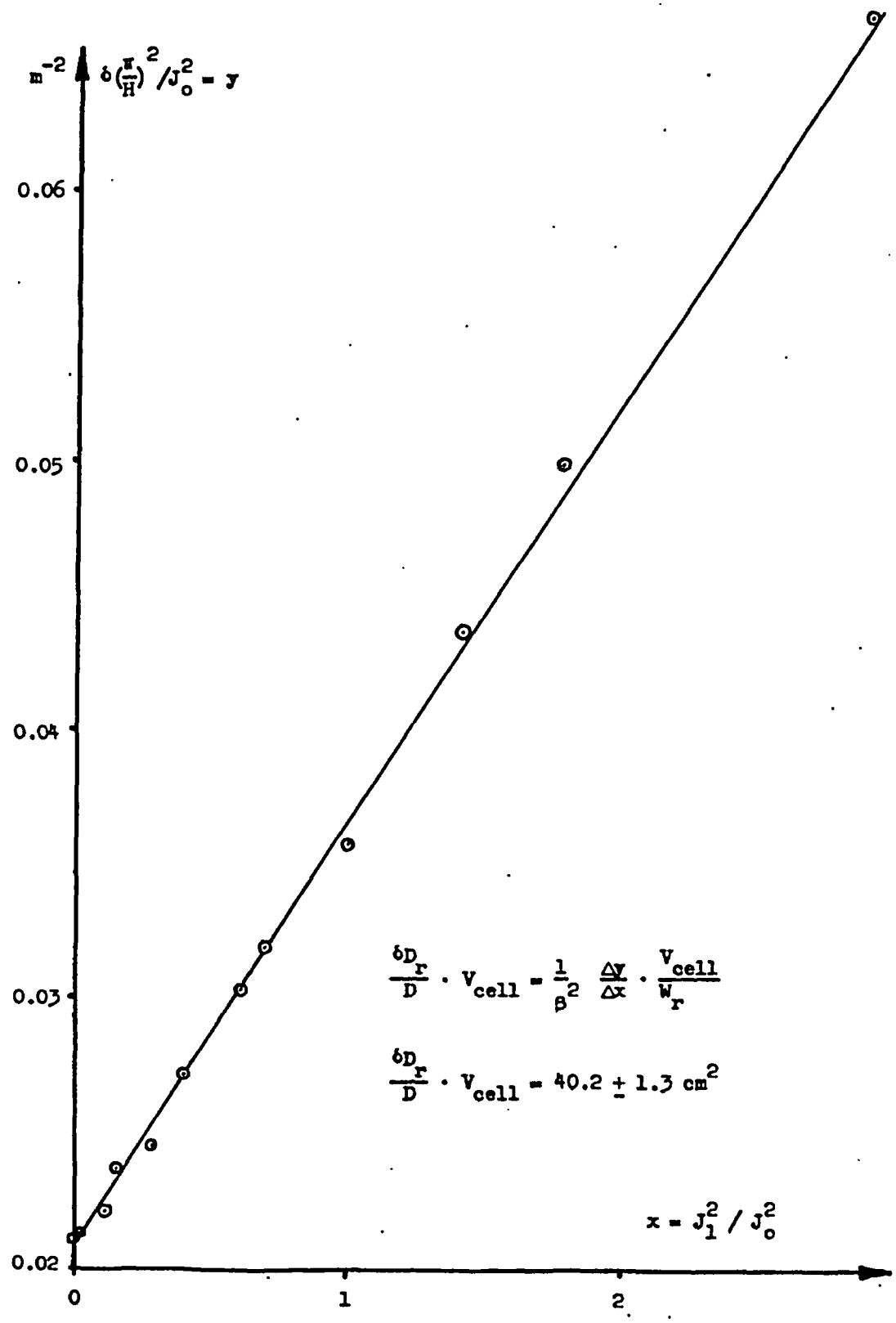

ESSELTE 4401

	The relative change of the diffusion coefficient due to coolant loss versus pitch.	FFR-113 Fig. 8

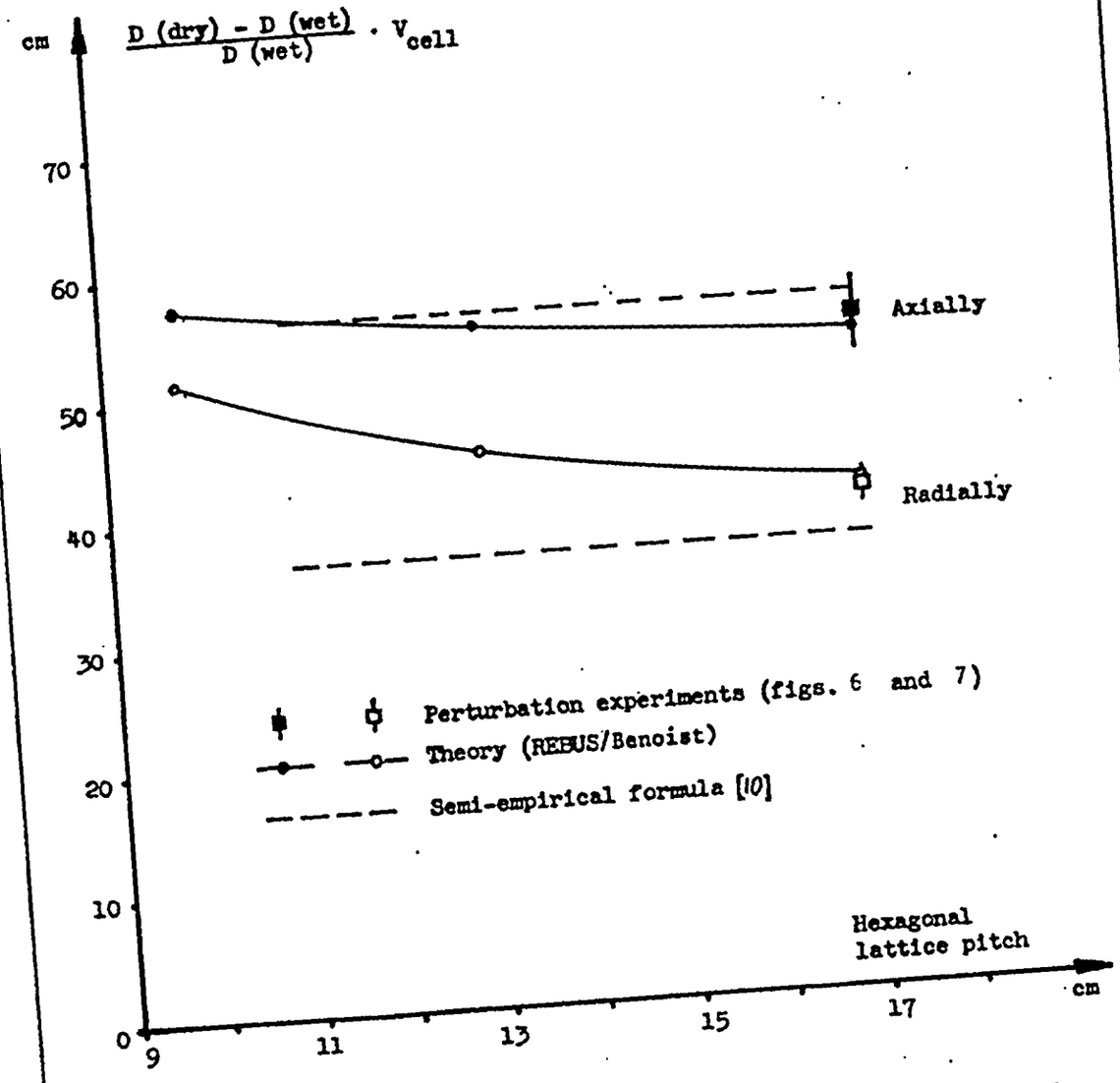

ESSELTE 4401

	Cell definitions used for the substitutions of ThO_2 fuel assemblies in the U metal rod lattices.	FFR-113 Fig. 9

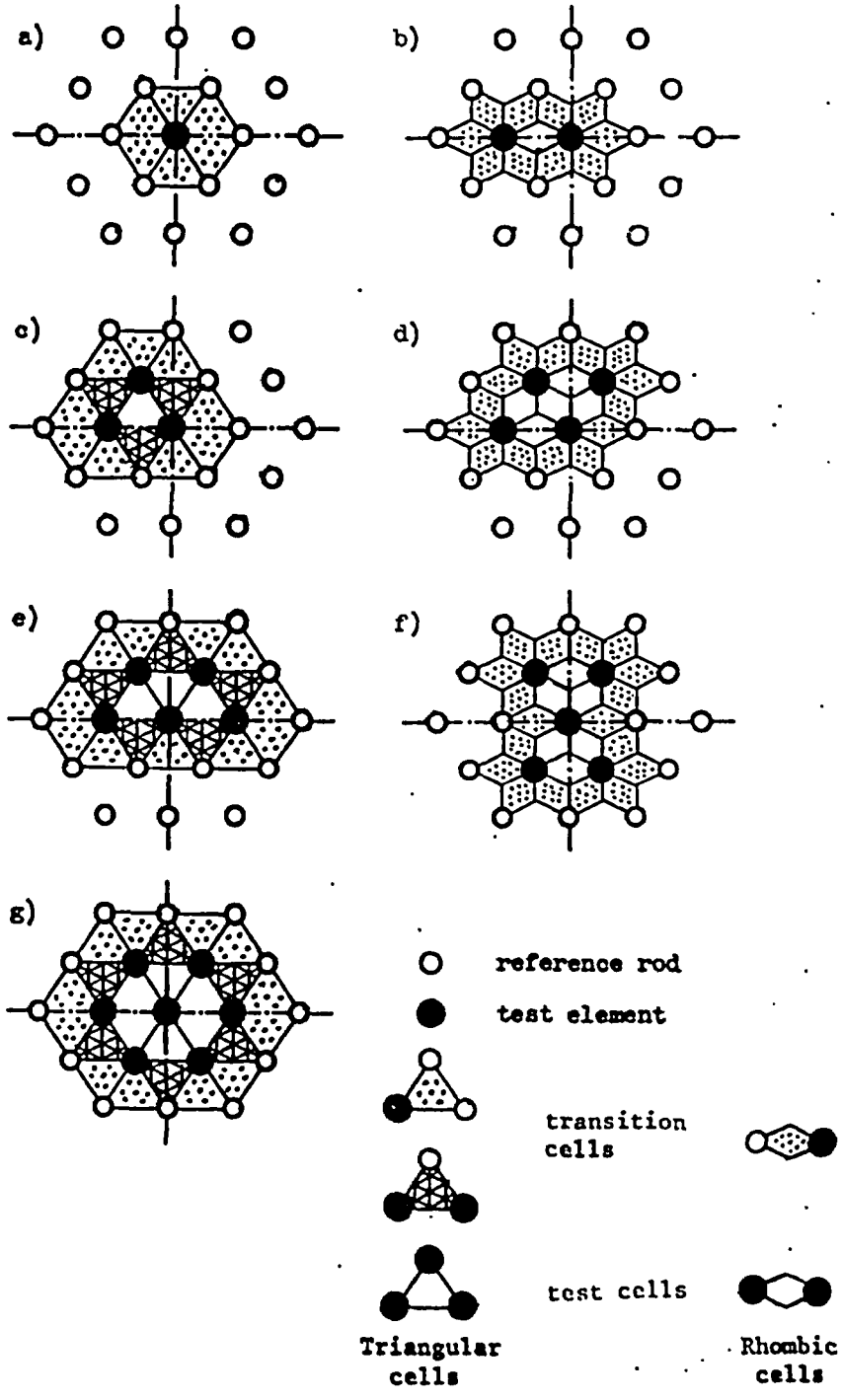

ESSELTE 4401

	Change of critical height versus number of substituted ThO_2 elements	FFR-113 Fig. 10

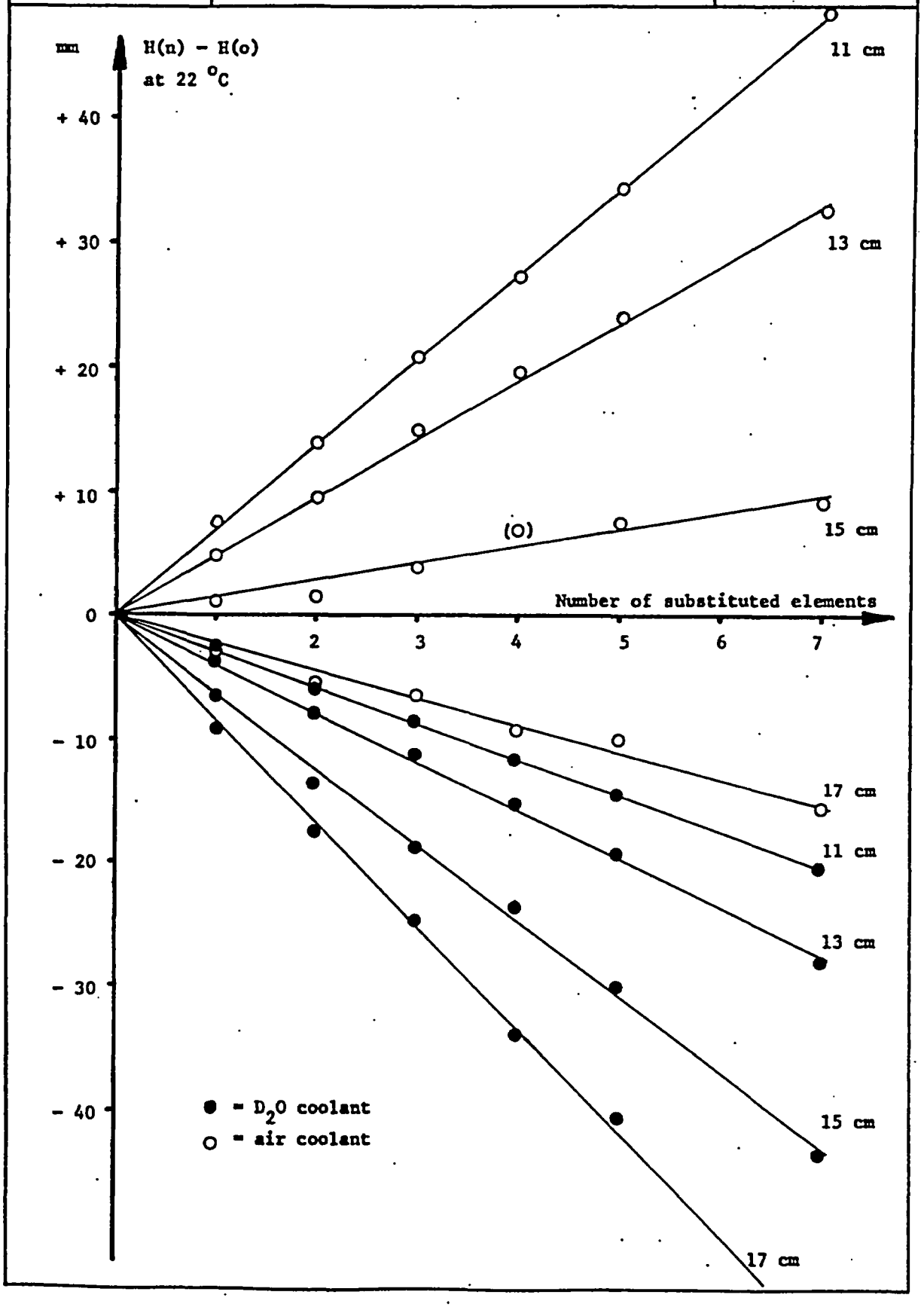

ESSELTE 4401

	Graphical representation of the perturbation analysis of the progressive substitutions with $ThO_2/U^{235}O_2$ clusters	FFR-113
		Fig. 11

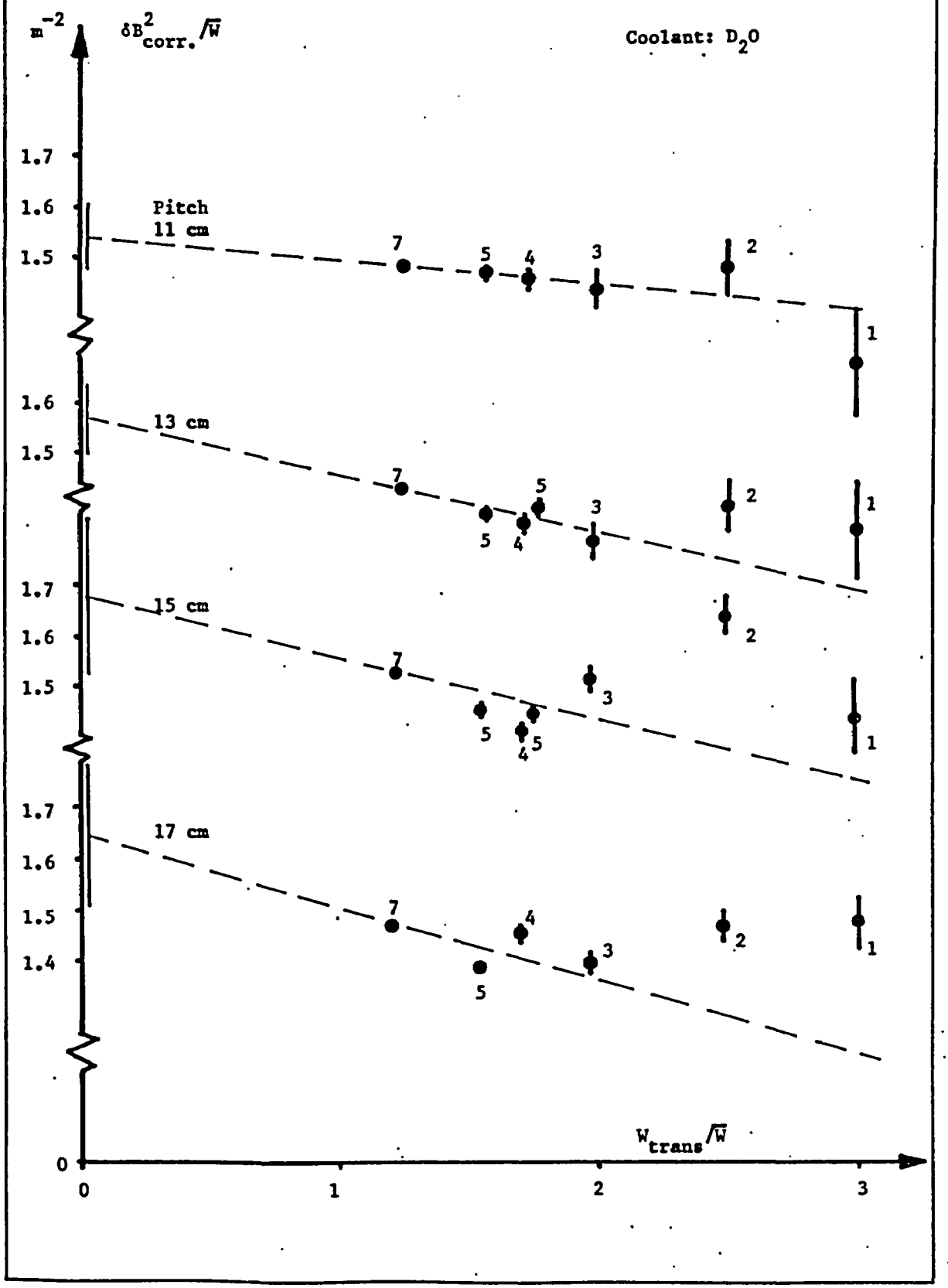

ESSELTE 4401

	Experimental buckling values including those of the transition regions versus lattice pitch	FFR-113 Fig. 12

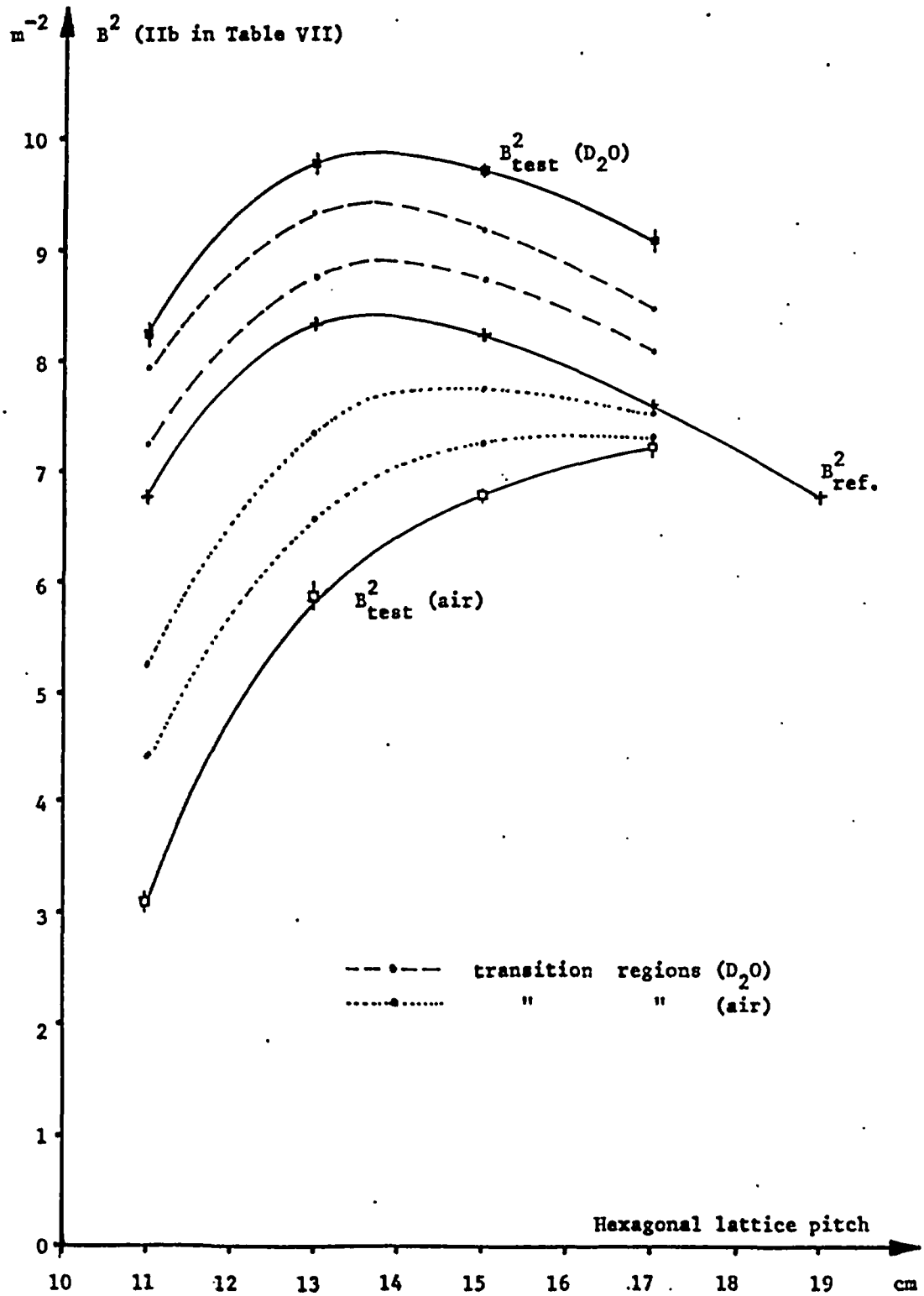

732501-113FA4
ESSELTE
4401

	Theoretical and experimental buckling values of the ThO_2 elements versus lattice pitch with the coolant as parameter	FFR-113 Fig. 13

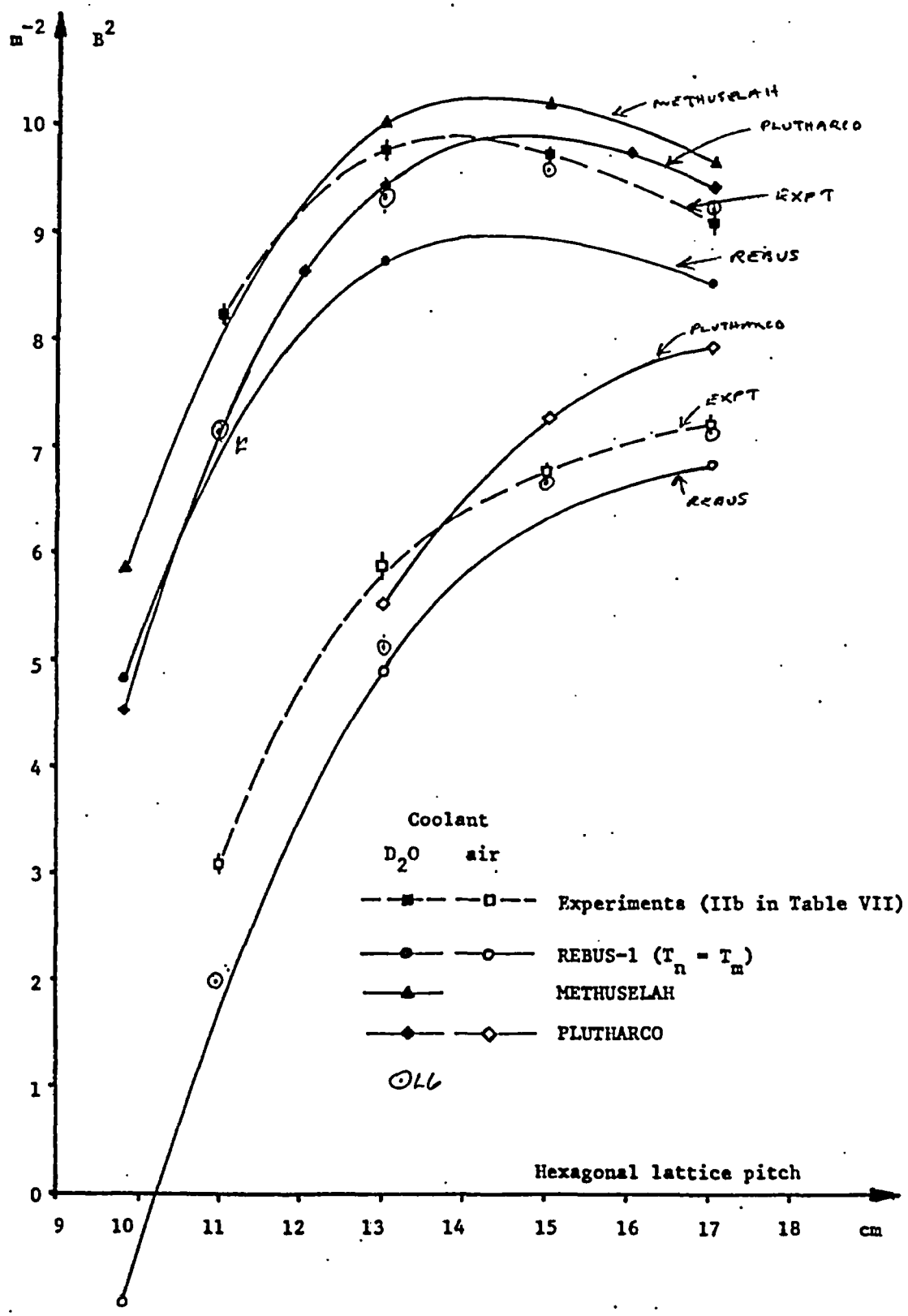

ESSELTE 4401

The buckling difference between water-cooled and air-cooled ThO_2 elements versus lattice pitch.

FFR-113

Fig. 14

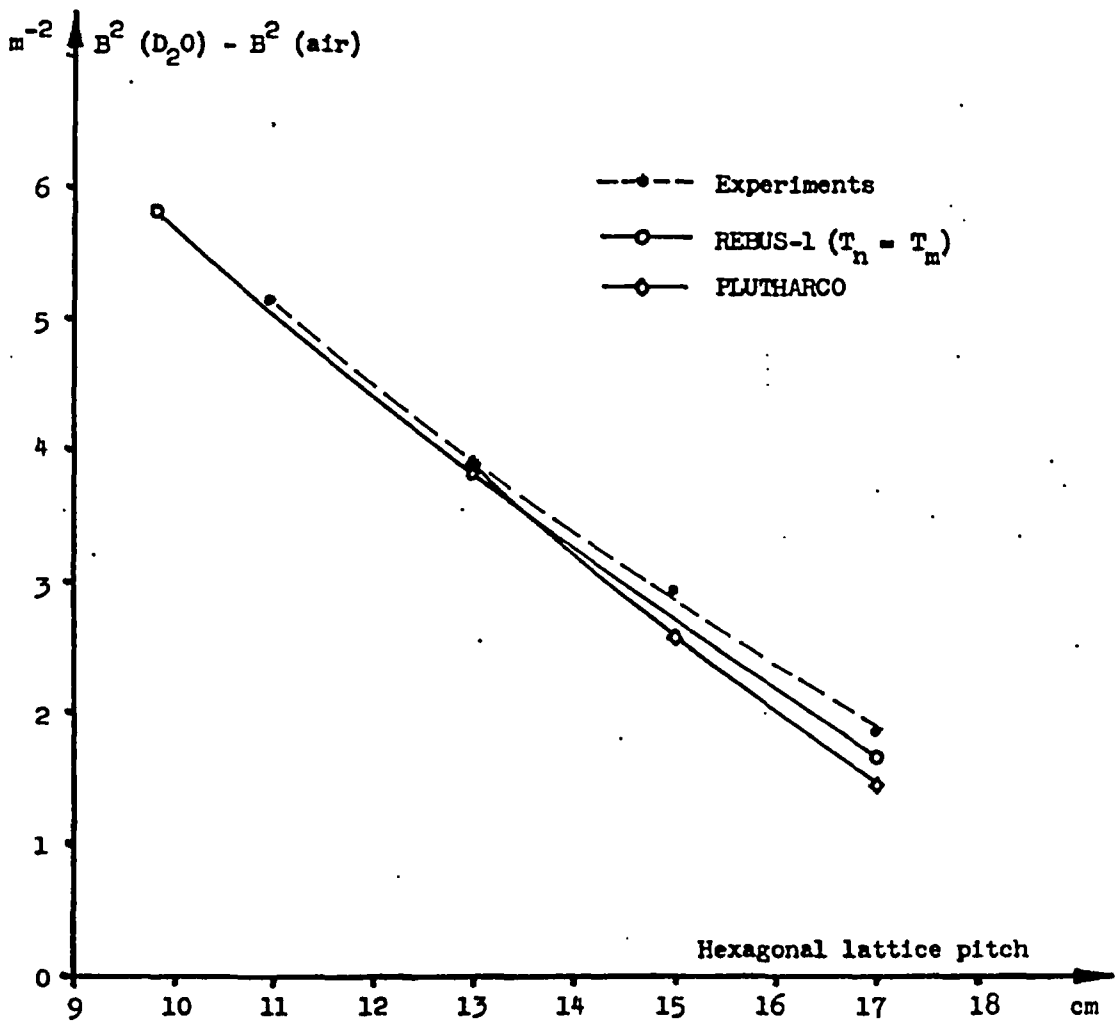

ESSELTE 4401

	Axial distribution measured with copper foils in the fuel stringers. 13 cm lattice with D_2O coolant	FFR-113
		Fig. 15

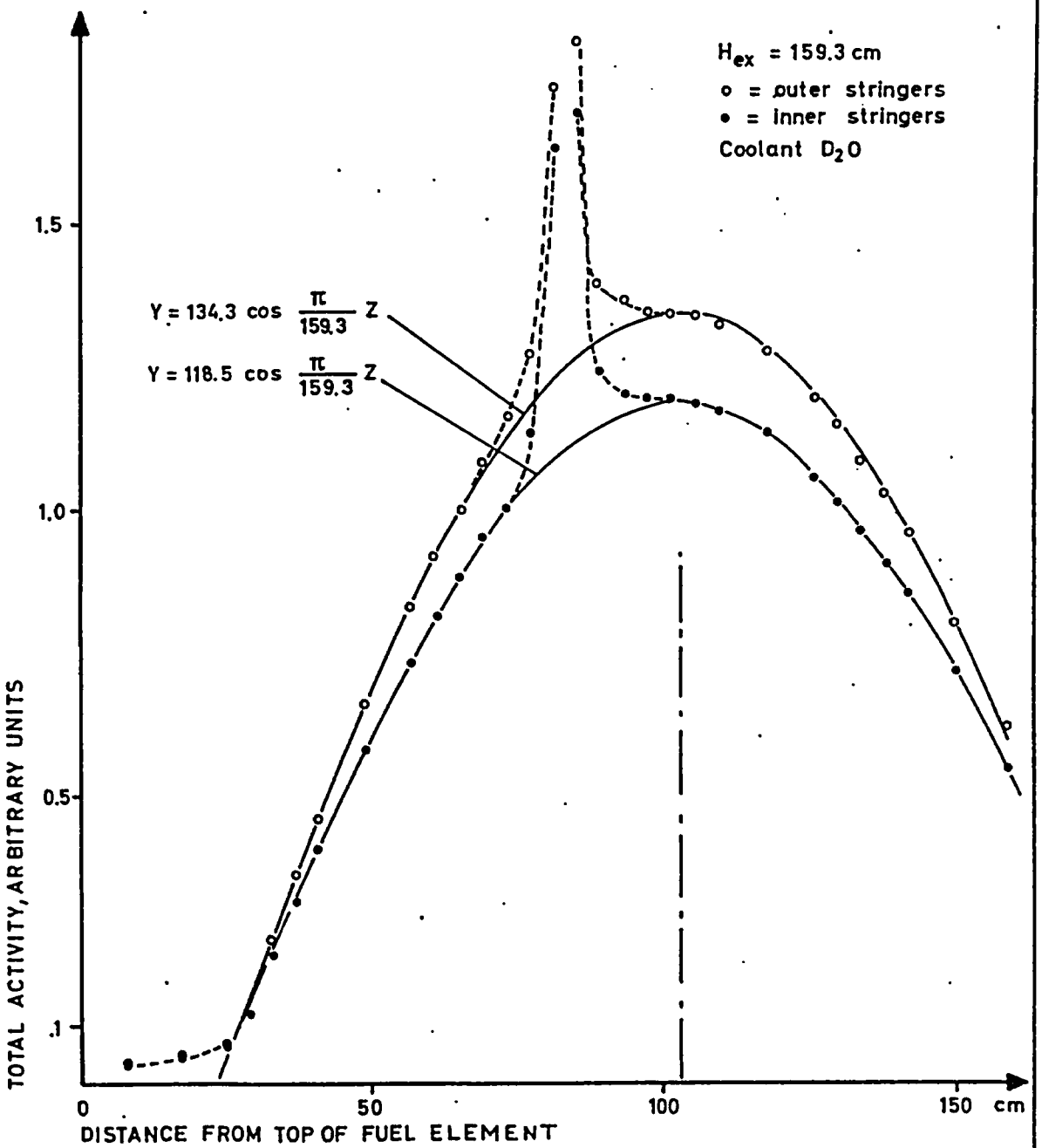

733501-113 A4
ESSELTE 4401

	Axial distribution measured with copper foils in the fuel stringers. 13 cm lattice with air coolant	FFR-113
		Fig. 16

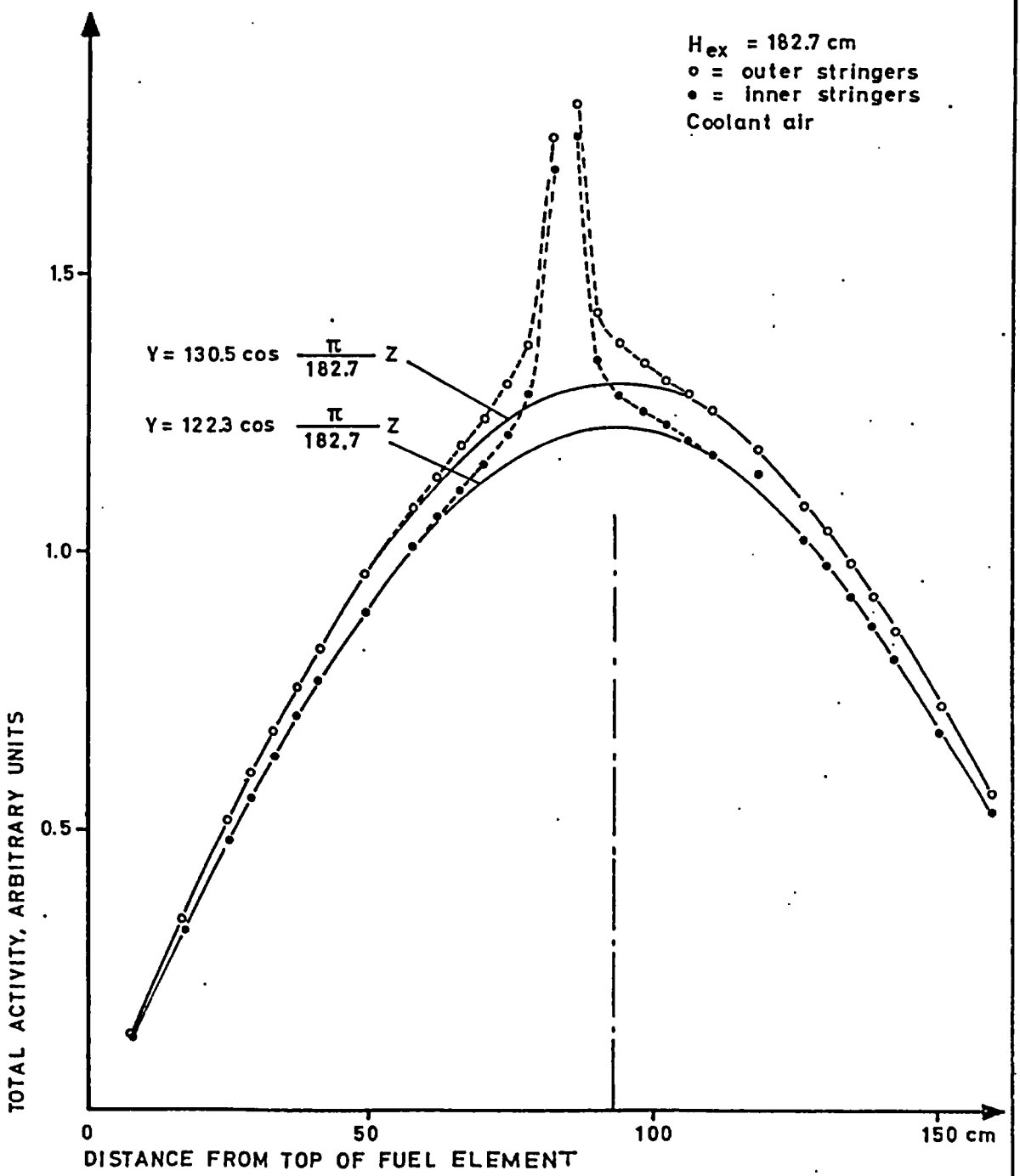

732501.113 A4
ESSELTE 4401

	The peaking factor Q versus axial position Coolant: D_2O	FFR-113 Fig. 17

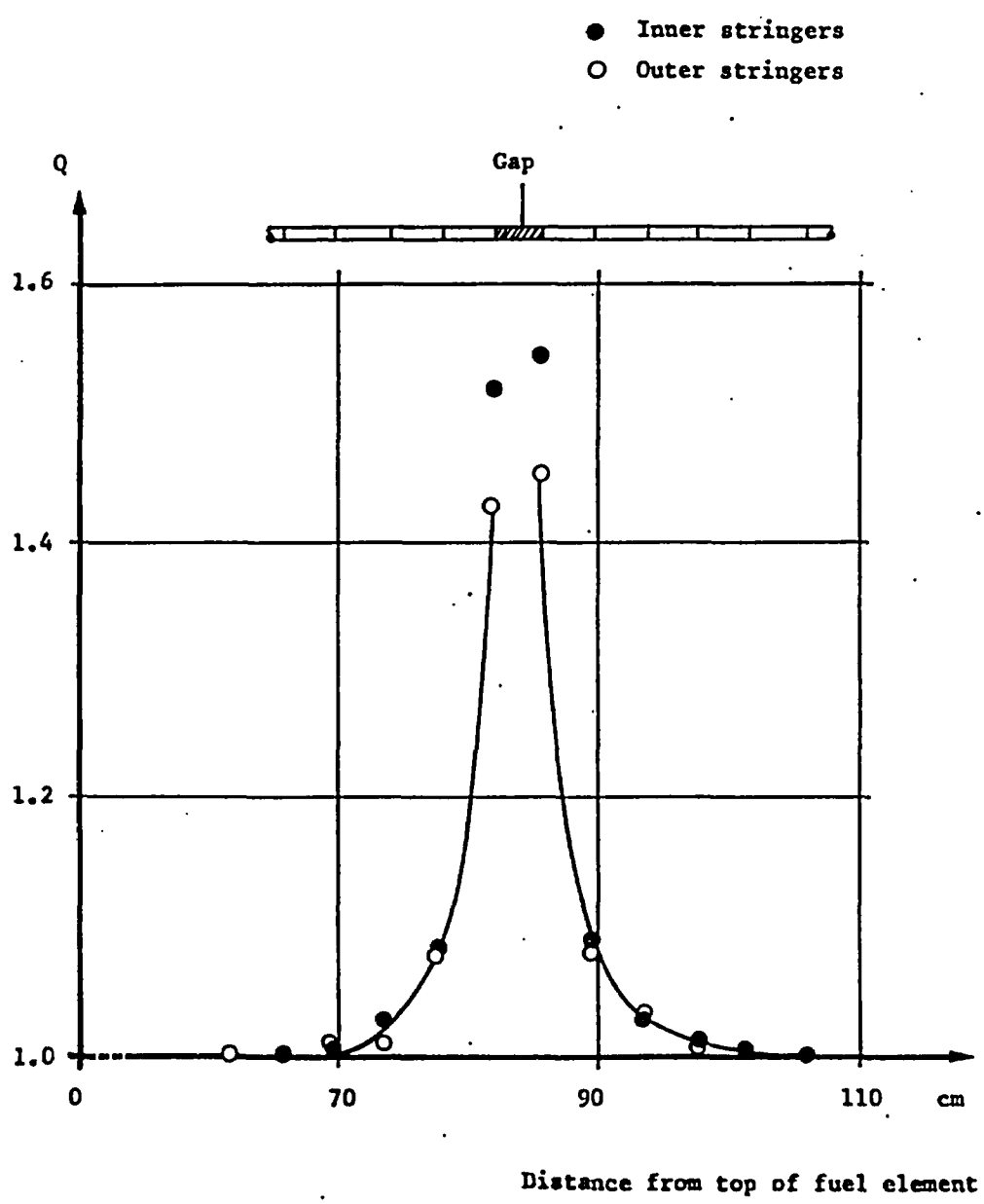

ESSELTE 4401

	The peaking factor Q versus axial position Coolant: Air	FFR-113 Fig. 18

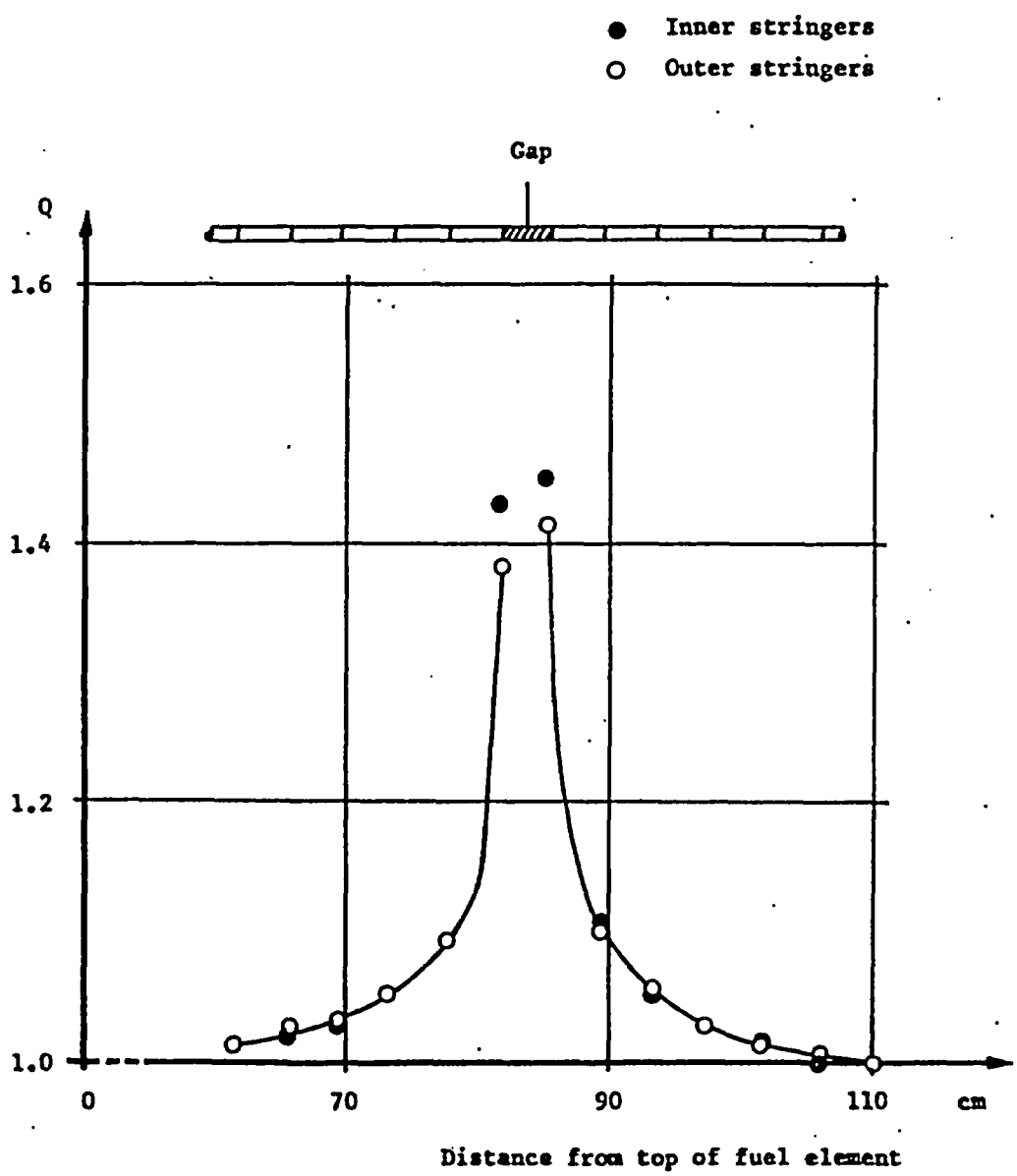

ESSELTE 4401

	Calculated axial flux distribution in the central and outer pins for the 13 cm pitch with D_2O coolant	FFR-113 Fig. 19

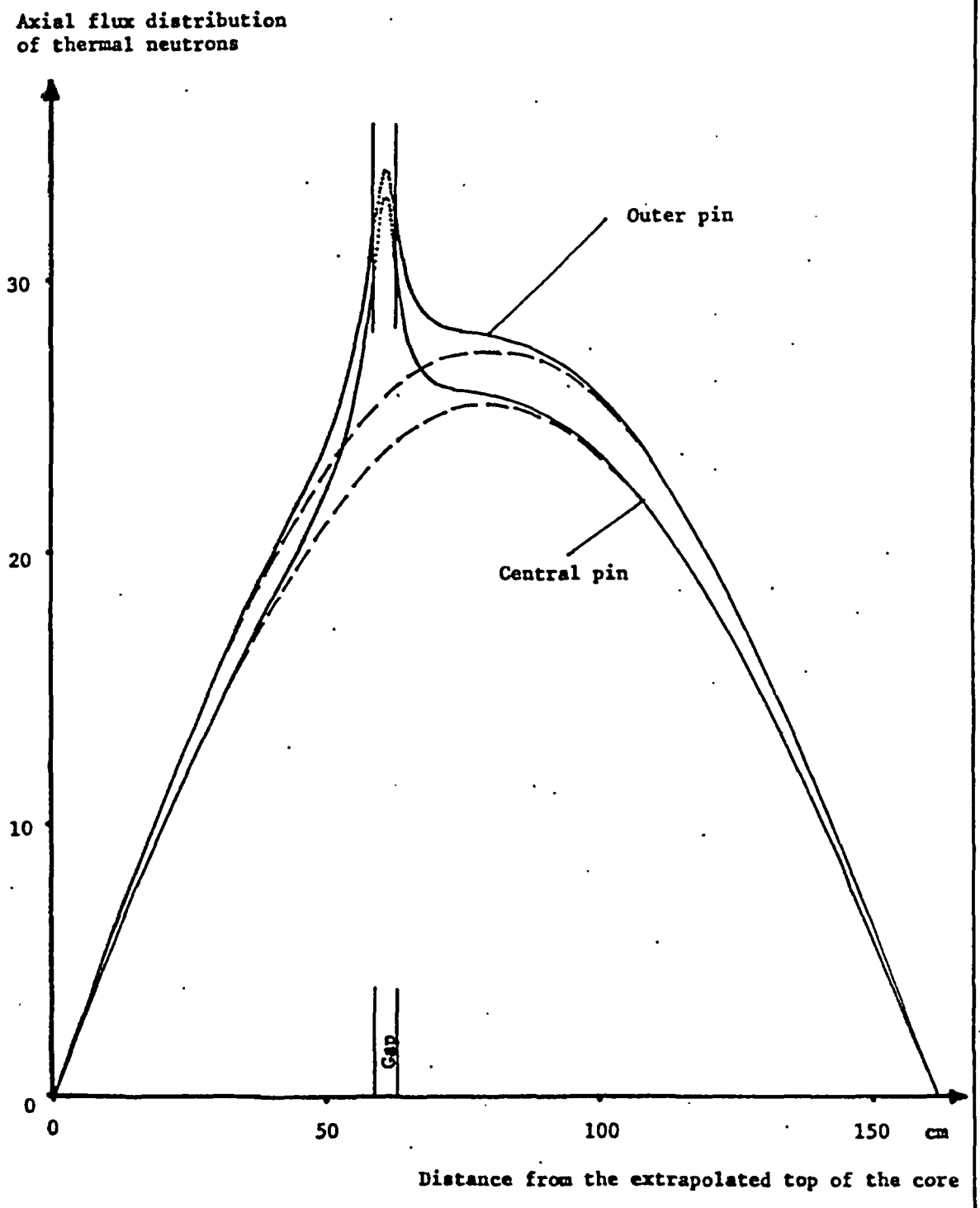

732501-113A4
ESSELTE
4401

	The epithermal spectrum index $P\ r\sqrt{T_n}$ in the 13 cm and 17 cm lattices versus $V_{fuel}\ \Sigma_{fuel}/V_m\ \Sigma_{nat}$	FFR-113 Fig. 20

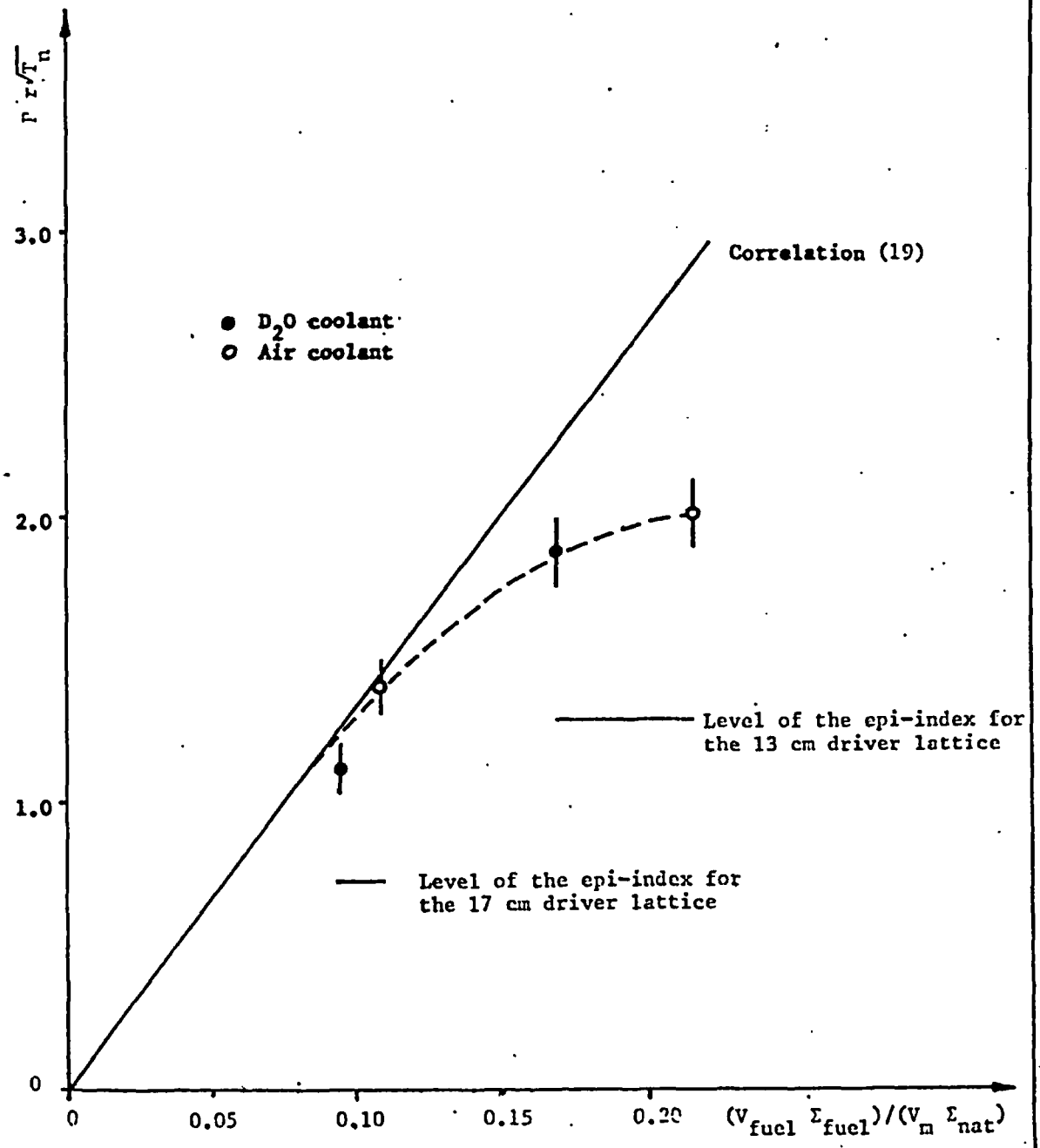

722501-113 A4
ESSELTE 4401

	Study of thermal column correction. Schematic loading diagram for samples	FFR-113 Fig. 21

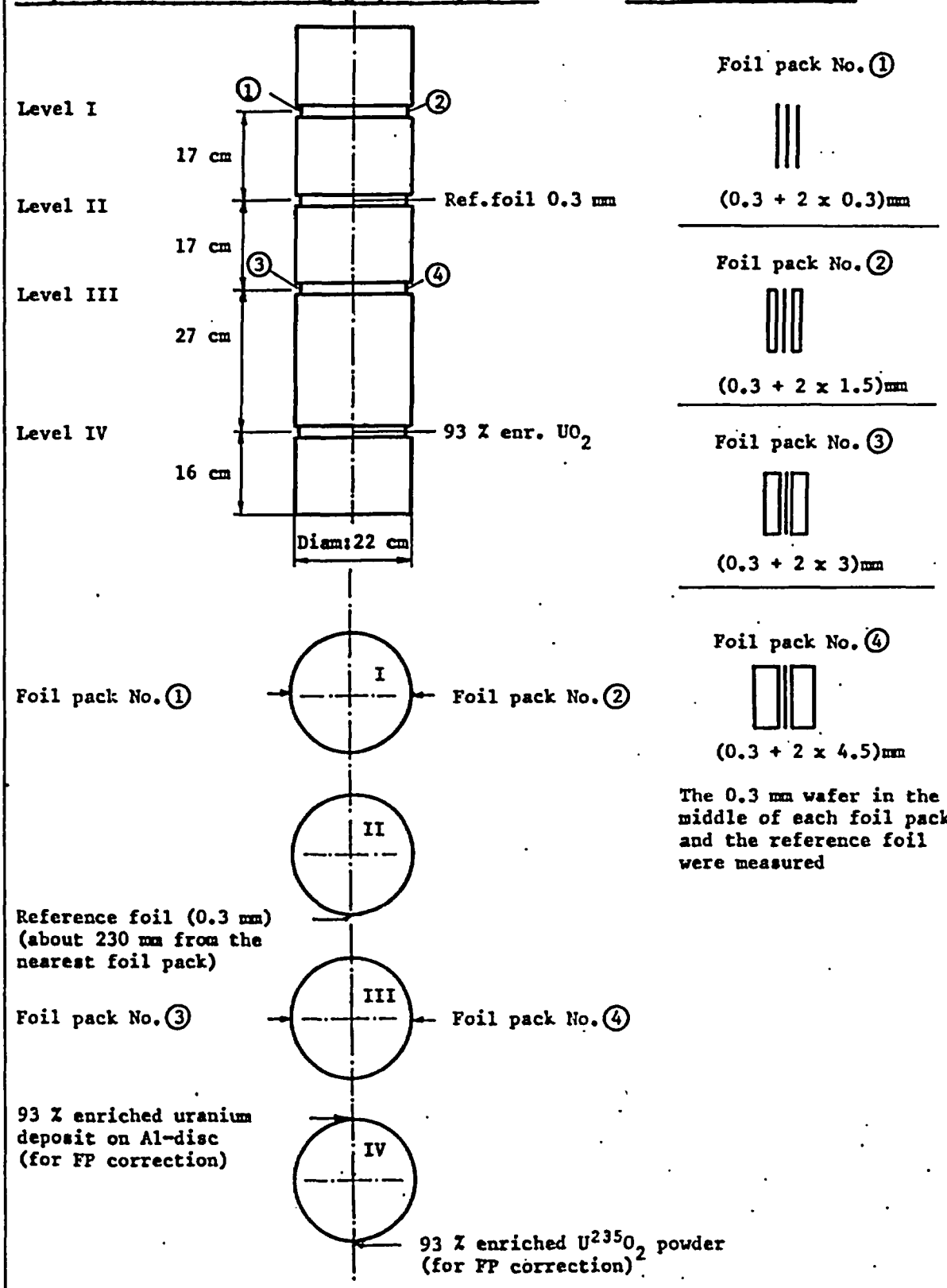

ESSELTE
4401

	Study of thermal column RCR* versus total thickness of foil pack	FFR-113 Fig. 22

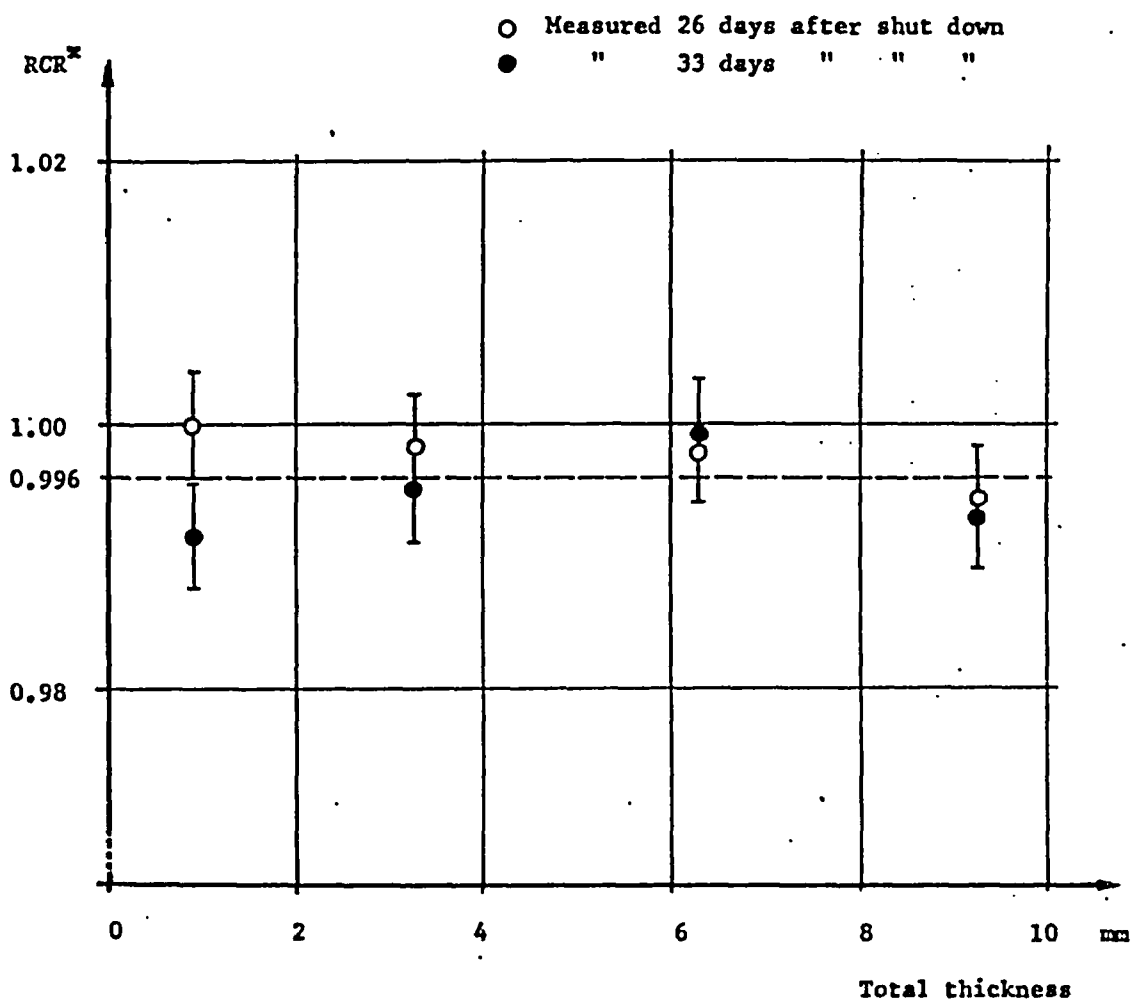

ESSELTE
4401

	FP correction and natural background activity (in % of total activity) measured versus time after shut down	FFR-113 Fig. 23

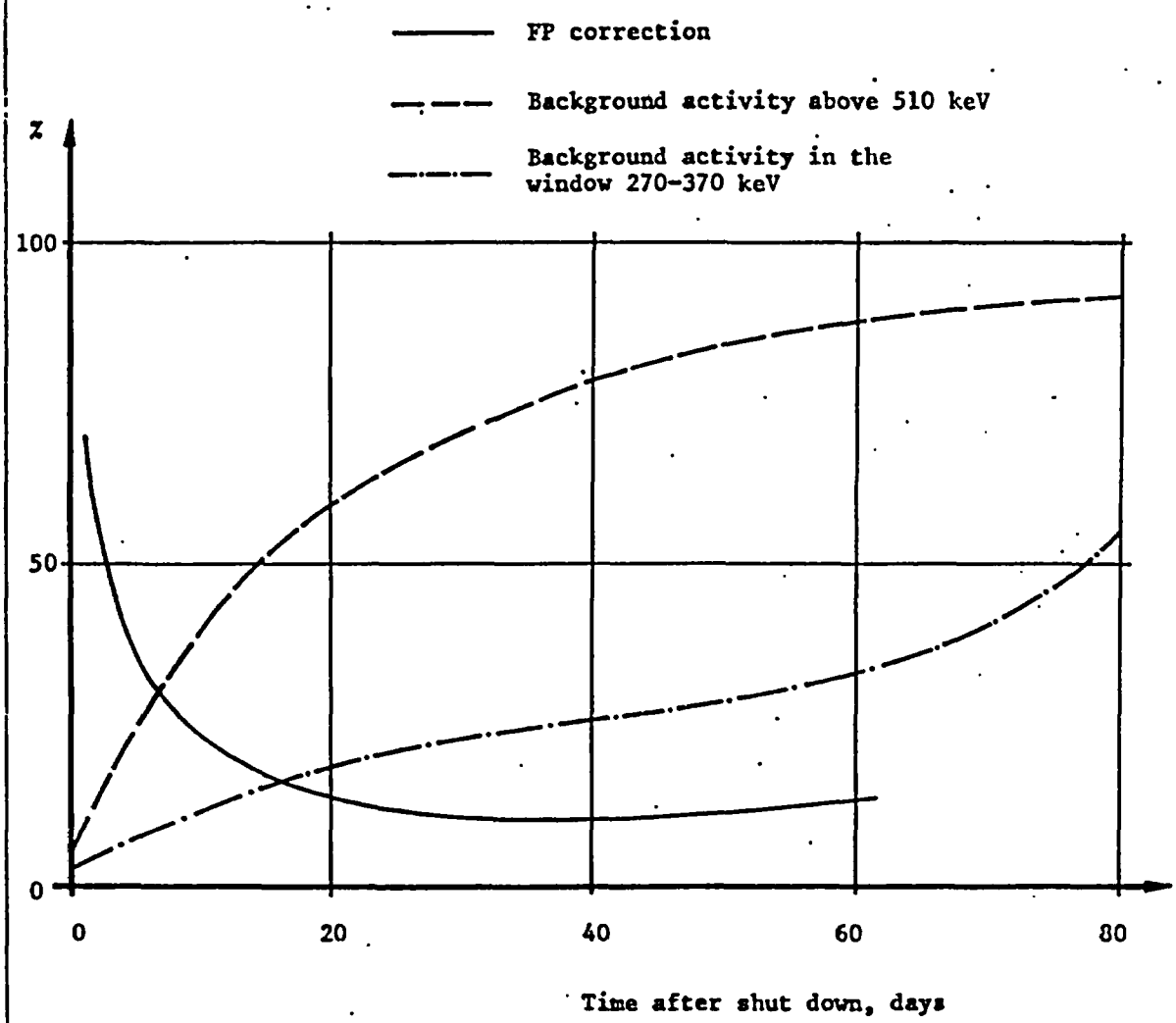

ESSELTE 4401

	$(RCR^{*}-1)$ versus $(V_{fuel}\Sigma_{fuel})/V_m\Sigma_{nat})$ Comparison between theoretical and measured values	FFR-113 Fig. 24

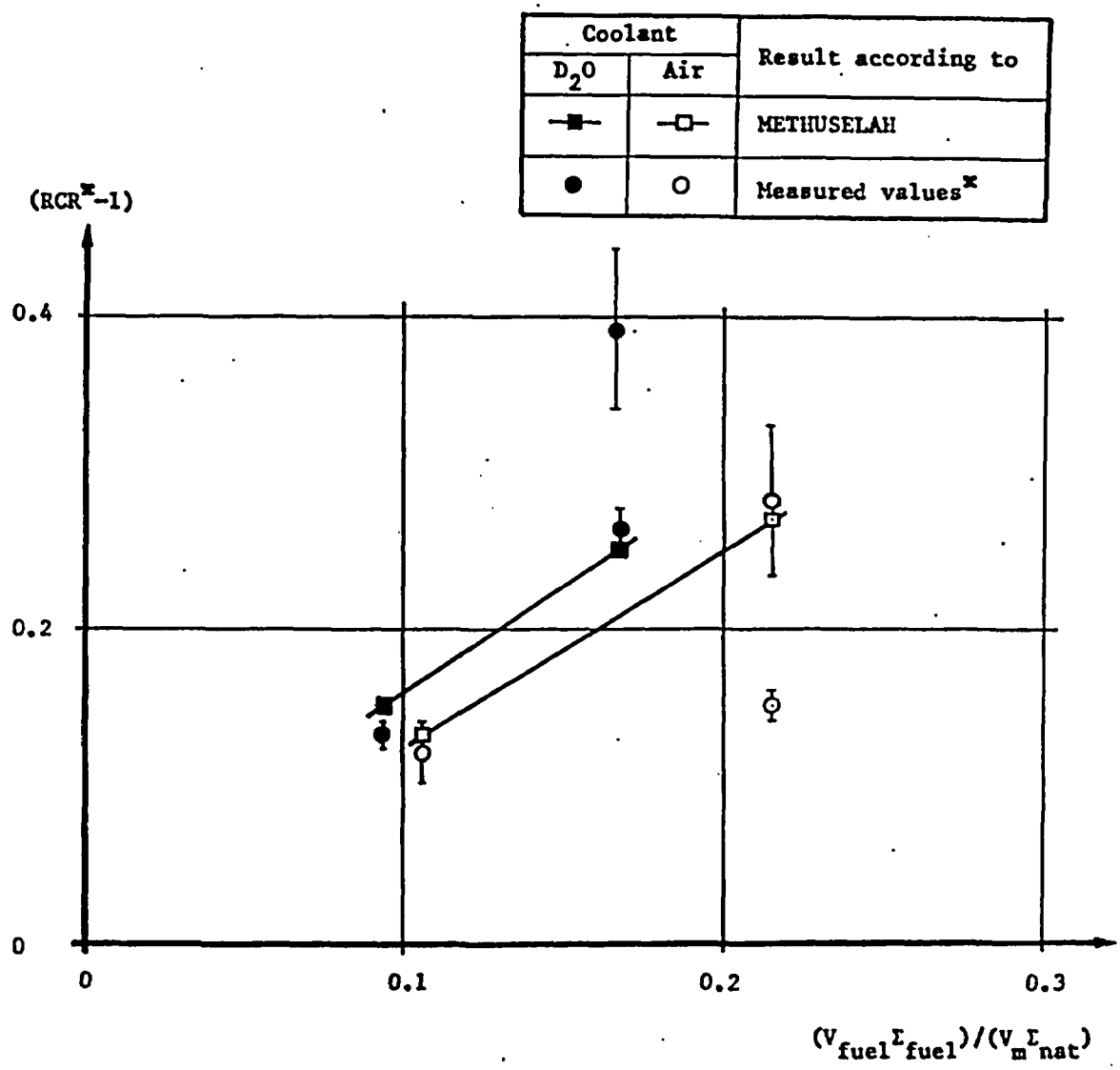

* Uncorrected for non-asymptotic spectral conditions